COPY 1 3

REPORT No.: FAA-RD-74-125, III-I

CORE ENGINE NOISE CONTROL PROGRAM

Volume III, Supplement I - PREDICTION METHODS

FAA WJH Technical Center
00026776

J. J. Emmerling

AIRCRAFT ENGINE GROUP
GENERAL ELECTRIC COMPANY
CINCINNATI, OHIO 45215

LIBRARY
SEP 25 '76

March 1976

FINAL REPORT

Document is available to the public through the
National Technical Information Service,
Springfield, Virginia 22151

Prepared for

U.S. DEPARTMENT OF TRANSPORTATION
FEDERAL AVIATION ADMINISTRATION
Systems Research & Development Service
Washington, D.C. 20590

NOTICE

This document is disseminated under the sponsorship of the Department of Transportation in the interest of information exchange. The United States Government assumes no liability for its contents or use thereof.

1. Report No.	2. Government Accession No.	3. Recipient's Catalog No.
FAA-RD-74-125, III-I		

4. Title and Subtitle	5. Report Date
Core Engine Noise Program Volume III, Prediction Methods -- Supplement I - Extension of Prediction Methods	March 1976
	6. Performing Organization Code
7. Author(s) J.J. Emmerling, S.B. Kazin (Program Technical Director) R.K. Matta (Editor)	8. Performing Organization Report No. R76AEG305
9. Performing Organization Name and Address Advanced Engineering and Technology Programs Department General Electric Company Aircraft Engine Group Evendale, Ohio 45215	10. Work Unit No. Dept. 36310
	11. Contract or Grant No. DOT-FA72WA-3023
12. Sponsoring Agency Name and Address U.S. Department of Transportation Federal Aviation Administration Systems Research and Development Service Washington, D.C. 20590	13. Type of Report and Period Covered Final June 1974-May 1975
	14. Sponsoring Agency Code

15. Supplementary Notes Volume I - Identification of Component Noise Sources, FAA-RD-74-125, I.
Volume II - Identification of Noise Generation and Suppression Mechanisms, FAA-RD-74-125, II.
Volume II - Supplement I - Identification of Noise Generation and Suppression Mechanisms, FAA-RD-74-125, II-I.
Volume III- Prediction Techniques - FAA-RD-74-125, III.

16. Abstract

The core noise prediction technique described in Volume III was validated using several additional sets of engine data. The data included discernible core noise at high power settings and were derived from both General Electric and external tests, on engines by GE and other manufacturers. The three line power level prediction method was collapsed to single unified line prediction through addition of a turbine work extraction term to account for the low frequency noise attenuation due to turbine blading.

Data from combustor component tests were compared to engine noise levels and found to indicate significant attenuation of low frequency noise in propagation through turbine stages. An analytical method for predicting this low frequency noise attenuation is provided.

17. Key Words (Suggested by Author(s))	18. Distribution Statement
Core Noise, Combustor Noise, Core Engine Noise, Gas Turbine Noise, Internal Noise	Document is available to the public through the National Technical Information Service, Springfield, Virginia 22151

19. Security Classif. (of this report)	20. Security Classif. (of this page)	21. No. of Pages	22. Price*
Unclassified	Unclassified	53	

METRIC CONVERSION FACTORS

Approximate Conversions to Metric Measures

Symbol	When You Know	Multiply by	To Find	Symbol
		LENGTH		
in	inches	*2.5	centimeters	cm
ft	feet	30	centimeters	cm
yd	yards	0.9	meters	m
mi	miles	1.6	kilometers	km
		AREA		
in^2	square inches	6.5	square centimeters	cm^2
ft^2	square feet	0.09	square meters	m^2
yd^2	square yards	0.8	square meters	m^2
mi^2	square miles	2.6	square kilometers	km^2
	acres	0.4	hectares	ha
		MASS (weight)		
oz	ounces	28	grams	g
lb	pounds	0.45	kilograms	kg
	short tons (2000 lb)	0.9	tonnes	t
		VOLUME		
tsp	teaspoons	5	milliliters	ml
Tbsp	tablespoons	15	milliliters	ml
fl oz	fluid ounces	30	milliliters	ml
c	cups	0.24	liters	l
pt	pints	0.47	liters	l
qt	quarts	0.95	liters	l
gal	gallons	3.8	liters	l
ft^3	cubic feet	0.03	cubic meters	m^3
yd^3	cubic yards	0.76	cubic meters	m^3
		TEMPERATURE (exact)		
°F	Fahrenheit temperature	5/9 (after subtracting 32)	Celsius temperature	°C

*1 in = 2.54 (exactly). For other exact conversions and more detailed tables, see NBS Misc. Publ. 286, Units of Weights and Measures, Price $2.25, SD Catalog No. C13.10:286.

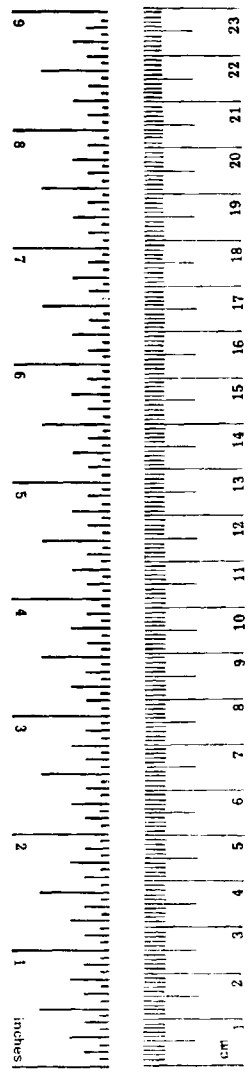

Approximate Conversions from Metric Measures

Symbol	When You Know	Multiply by	To Find	Symbol
		LENGTH		
mm	millimeters	0.04	inches	in
cm	centimeters	0.4	inches	in
m	meters	3.3	feet	ft
m	meters	1.1	yards	yd
km	kilometers	0.6	miles	mi
		AREA		
cm^2	square centimeters	0.16	square inches	in^2
m^2	square meters	1.2	square yards	yd^2
km^2	square kilometers	0.4	square miles	mi^2
ha	hectares (10,000 m^2)	2.5	acres	
		MASS (weight)		
g	grams	0.035	ounces	oz
kg	kilograms	2.2	pounds	lb
t	tonnes (1000 kg)	1.1	short tons	
		VOLUME		
ml	milliliters	0.03	fluid ounces	fl oz
l	liters	2.1	pints	pt
l	liters	1.06	quarts	qt
l	liters	0.26	gallons	gal
m^3	cubic meters	35	cubic feet	ft^3
m^3	cubic meters	1.3	cubic yards	yd^3
		TEMPERATURE (exact)		
°C	Celsius temperature	9/5 (then add 32)	Fahrenheit temperature	°F

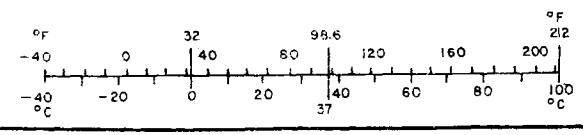

PREFACE

This report describes the work performed under the DOT/FAA Core Engine Noise Control Program (Contract DOT-FA72WA-3023). The original work under this contract is in Report Number FAA-RD-74-125, Volumes I,II, and III.

Supplements to Volumes II and III report additional work undertaken under this program after completion of the work reported in the original three volumes.

The objectives of the program were:

- Identification of component noise sources of core engine noise (Phase I).
- Identification of mechanisms associated with core engine noise generation and noise reduction (Phases II and III).
- Development of techniques for predicting core engine noise in advanced systems for future technology aircraft (Phase IV).
- Extension of the core noise prediction (Phase V).
- Update of the core engine noise control effort (Phase VI).

The objectives were accomplished in six phases as follows:

- Phase I - Analysis of engine and component acoustic data to identify potential sources of core engine noise and classification of the sources into major and minor categories.
- Phase II - Identification of the noise generating mechanism associated with each source through a balanced program of:

  Analytical studies

  Component and model tests

  Acoustic evaluation of data from existing and advanced engine systems.
- Phase III - Identification of noise reduction mechanisms for each source through a program with elements similar to Phase II.
- Phase IV - Development of improved prediction techniques incorporating the results obtained during the preceding two phases.

- Phase V - Analysis of low frequency noise transmission through turbine blade rows and addition of engine and component data to the prediction method for core noise.

- Phase VI - Analytical studies of turbine source noise suppression and parametric trends in turbine tone/jet stream interaction; an experimental study of compact low frequency noise suppressors and a prediction model update.

The work accomplished is reported in five volumes corresponding respectively to the five objectives stated above.

- Volume I - Identification of Component Noise Sources (FAA-RD-74-125, I).

- Volume II - Identification of Noise Generation and Suppression Mechanisms (FAA-RD-74-125, II).

- Volume III - Prediction Methods (FAA-RD-125, III).

- Volume III Supplement I - Extension of Prediction Methods. (FAA-RD-74-125, III-I)

- Volume II Supplement I - Extension to Identification of Noise Generation and Suppression Mechanisms. (FAA-RD-74-125, II-I)

A visual representation of the overall program and report organization is shown on page v and vi.

This volume documents the results of the Phase V activity which extended the core noise prediction technique through:

1) Examination of additional engine data to validate the prediction method.

2) Re-evaluation of the prediction at high power settings through examination of engine data.

3) Analytical determination of turbine low frequency noise attenuation in order to add component data to the engine prediction lines.

CORE ENGINE NOISE CONTROL PROGRAM OVERALL REPORT ORGANIZATION

Contract Phase		Contract Documentation
Phase I	Volume I	Identification of Component Noise Sources FAA-RD-74-125,I
Phase II and Phase III	Volume II	Definition of Mechanisms of Noise Generation Definition of Mechanisms of Noise Reduction FAA-RD-74-125,II
Phase IV	Volume III	Development of Prediction Techniques FAA-RD-74-125,III

CORE ENGINE NOISE CONTROL PROGRAM OVERALL REPORT ORGANIZATION

Contract Phase		Contract Documentation
Phase V	Volume III, Supplement I	Extension of the Core Noise Prediction Technique FAA-RD-74-125, III-I
Phase VI	Volume II, Supplement I	Extension to the Definition of the Mechanisms of Noise Generation and Suppression FAA-RD-74-125, II-I

TABLE OF CONTENTS

Section		Page
	PREFACE	iii
	SUMMARY	xi
1.0	INTRODUCTION	1
2.0	ADDITIONAL ENGINE DATA	2
	2.1 JT8D NASA Refan Engine	2
	2.2 Garrett Turboshaft Engine	6
	2.3 NASA TF34 Engine Test	8
	2.4 Boeing Data	8
3.0	ENGINE HIGH POWER SETTING EVALUATION	13
	3.1 The Spectrum Level	13
	3.2 Spectral Shape at High Power Settings	14
	3.3 Engine High Power Setting Directivity	19
4.0	ADDITIONAL COMPONENT DATA	20
	4.1 Component Combustor Spectra	20
	4.2 Component Combustor Power Level	24
	4.3 Turbine Blade Row Attenuation	24
5.0	CONCLUSIONS	31
	REFERENCES	32
APPENDICES		
	A. THE ENGINE LOW FREQUENCY CORE NOISE PREDICTION	33
	B. PROGRAM LISTING - PREDICTION OF BLADE ROW ATTENUATION	37

List of Illustrations

Figure No.		Page
2-1	Comparison of Predicted and Measured Spectral Shapes of Low Frequency Core Noise.	3
2-2	Comparison of Predicted and Measured Polar Directivities for the JT8D-109 Refan Engine.	4
2-3	Comparison of Predicted and Measured Low Frequency Core Noise Levels for the NASA JT8D-109 Refan Engine.	5
2-4	Spectral Shape Comparison of Turboshaft Data.	7
2-5	Turboshaft 400 Hz Directivity.	7
2-6	Comparison of Turboshaft Power Levels To The Prediction Parameter.	9
2-7	TF34 Spectral Comparison Using Engine Center-Line Microphones.	10
2-8	Comparison of GE and NASA TF34 Engine Data.	11
2-9	Comparison of Boeing Data With GE Procedure.	12
3-1	Engine "A" Quiet Engine Program at 70% Fan Speed.	15
3-2	The Limit of Jet Noise Determined by the Exponent of the Exhaust Velocity.	16
3-3	Comparison of QEP "A" Engine Spectrum.	17
3-4	Engine "A" Core Noise Levels for Power Settings From Idle to Takeoff Speeds.	18
4-1	Power Level (Corrected From 16 Foot High to 2 Foot High Microphones), F101 Component Combustor.	21
4-2	Power Level (Corrected From 16 Foot High to 2 Foot High Microphones) CF6 Component Combustor.	21
4-3	Comparison of an Engine to Component Test Configuration.	22

List of Illustrations (concluded)

Figure No.		Page
4-4	Comparison of Six Combustors With The Downstream Probe At a Constant Fuel-Air Ratio of 0.0245.	23
4-5	Component Combustor Power Level Vs. Prediction Parameter.	25
4-6	Geometry of Incident Wave on a Stage Element.	27
4-7	Stage 1 High Pressure Turbine, Low Frequency Attenuation.	28
4-8	Stage 5 Low Pressure Turbine, Low Frequency Attenuation.	29
A-1	Correlation for Core Noise Power Level.	35
A-2	Core Noise Prediction Spectra.	36
A-3	Average Value of Directivity.	36

NOMENCLATURE

V	Velocity
$\dot{W}$	Air flow rate
T	Temperature
θ	Angle
ρ	Density
P	Pressure
M	Mach number
Max	Maximum

SUBSCRIPTS

0	Standard day ambient condition
3	Entering the combustor
4	Leaving the combustor
5	Leaving the low pressure turbine
8	Leaving the exhaust nozzle
i	Incidence (Acoustic Wave)

SUMMARY

The DOT/FAA Core Noise Prediction Model was modified to include the results of additional engine noise data. The three line prediction method was improved to a single prediction line method by utilizing a turbine work extraction factor. The improvement in the prediction model has yielded a correlation within ±2 dB for all data analyzed to date.

A total of thirteen sets of engine data were evaluated. Three of these sets were from non-General Electric tests: a JT8D-109 (P&WA) low bypass ratio turbofan, a TPE 331-201 (Garrett) turboshaft engine and a TF34 (NASA) high bypass turbofan. The spectra and directivity of all three sets agree with the prediction method of Volume II, Section 3. The turboshaft engine and the TF34 power levels also agreed with this prediction; however, the low bypass ratio turbofan was 6 dB higher than the levels predicted from high bypass ratio engine data. It is suggested that the higher levels of combustor noise are due to lower turbine blade row attenuation for this low bypass engine. When the blade row attenuation is accounted for by means of a turbine work extraction term, the JT8D-109 data appear to be within 1 dB of the prediction line. In addition, the Boeing Company provided four other sets of high bypass ratio turbofan engine data, which were within ±2 dB of the prediction line.

An evaluation of the Quiet Engine Program Fan "A" engine data was performed over the entire operating range. The data were found to agree with both the overall power level and the spectral shape used in the prediction method for power settings up to and including takeoff.

The combustor component spectra were found to have the same shape as the prediction spectrum and the spectral envelope (see Volume II, Section 3). However, the frequency of the peak level was found to vary from 200 to 800 Hz; whereas the prediction for engine core noise sets the peak level at 400 Hz ± a one-third octave band. It is suspected that the influence of the engine components along the propagation path and termination of the nozzle have an influence on both the radiated spectrum shape and peak frequency, which would account for the peak frequency differences.

The overall power levels of the component combustors were significantly higher than the engine data for any value of the prediction parameter. This is most probably due to the attenuation occurring in passage through the downstream turbine blade rows. A theoretical analysis for turbine blade row attenuation successfully models this phenomenon, but over predicts the attenuation as indicated by the comparison of the component and engine data. Currently, an in-depth program to investigate turbine blade row attenuation is underway (NAS3-19435 and DOT-FA75WA-3688). The results of a parametric study conducted with this analysis indicated that the low frequency noise attenuation was a function of the work extraction by the turbine blade rows. The three line prediction method for core noise levels given in Volume II collapsed to a universal line when the engine data were normalized by the design point work extraction by the turbines.

SECTION 1.0

INTRODUCTION

A prediction for low frequency core engine noise was derived from an evaluation of available data as a part of Phase IV of the Core Engine Noise Program. This basic (Reference 1) prediction was modified to take into account the three hasic engine types, turbofan, turboshaft and turbojet. The correlation that was shown was based primarily on the low frequency data from the engines at low power setting.

The engine data available at the time was in many cases significantly influenced by jet noise at the higher power settings. Since the writing of that report, additional engine data have become available to enter into the correlation. Some of these data permit evaluation of engine core noise at higher power settings.

The differences in the absolute level of the low frequency noise radiation from the three engine types has been attributed to the varying attenuation of combustor noise while propagating through the downstream turbine blade rows. An analysis to explain the phenomenon of attenuation of low frequency noise by turbine blade rows has become available and some results from that analysis are presented. The assumption of this attenuation mechanism permited addition of component data to the correlation. Two series of component tests are reported.

SECTION 2.0

ADDITIONAL ENGINE DATA

During the evaluation of core noise data presented in Volume III it was noted that several sets of additional engine data were forthcoming which were not available at the time of that report's publication. The engines were the NASA JT8D-109 Refan, a Garrett turboshaft and a TF34 high bypass turbofan. The results of these subsequent engine tests are presented here. In addition, the Boeing Company provided 6 data sets from turbofan engines for comparison with the prediction.

2.1 NASA JT8D-109 REFAN ENGINE

Low frequency core noise from a JT8D-109 refan engine has been evaluated by comparing this data to the core noise prediction.* Low frequency core noise is present for this engine over a range of lower power settings.

Figure 2-1 shows that the spectral shapes fall between the broader more conservative spectral envelope (Volume III, Figure 3.3-2) and the more narrow T64 spectrum which was found to be a good approximation of component combustor noise. Both of these spectra are peaked at 400 Hz, (however the peak could be one-third octave band higher or lower). The Refan data peaks between 400 and 500 Hz. The data indicates that there is a variation in the spectrum shape with angle. The refan spectra fall between the two suggested by the prediction method, however.

The predicted directivity peaks at 120°, and does not change shape with speed. The refan directivities are similar in shape, however the angle at which they peak changes from 130° to 110° as engine speed increases (Figure 2-2).

These variations in spectral shape and directivity are considered minor. The major variation of the JT8D-109 Refan occurs in level. The NASA data were provided in the form of peak OASPL versus percent fan speed, and on this basis the OASPL at 120° was found to be 6 dB higher (Figure 2-3) than the prediction for typical high bypass ratio turbofan engines used in the GE method. This level is almost as high as the turboshaft engines (which were 8 dB higher than turbofans). This difference in levels could possibly be due to either of two contributing factors. The first is that the "can"-type combustors employed in the JT8D-109 engine could possibly have generated higher levels. The core noise prediction was developed based on annular combustors. The second factor,

* These data were provided by E. Krejsa of NASA-LEWIS Research Center.

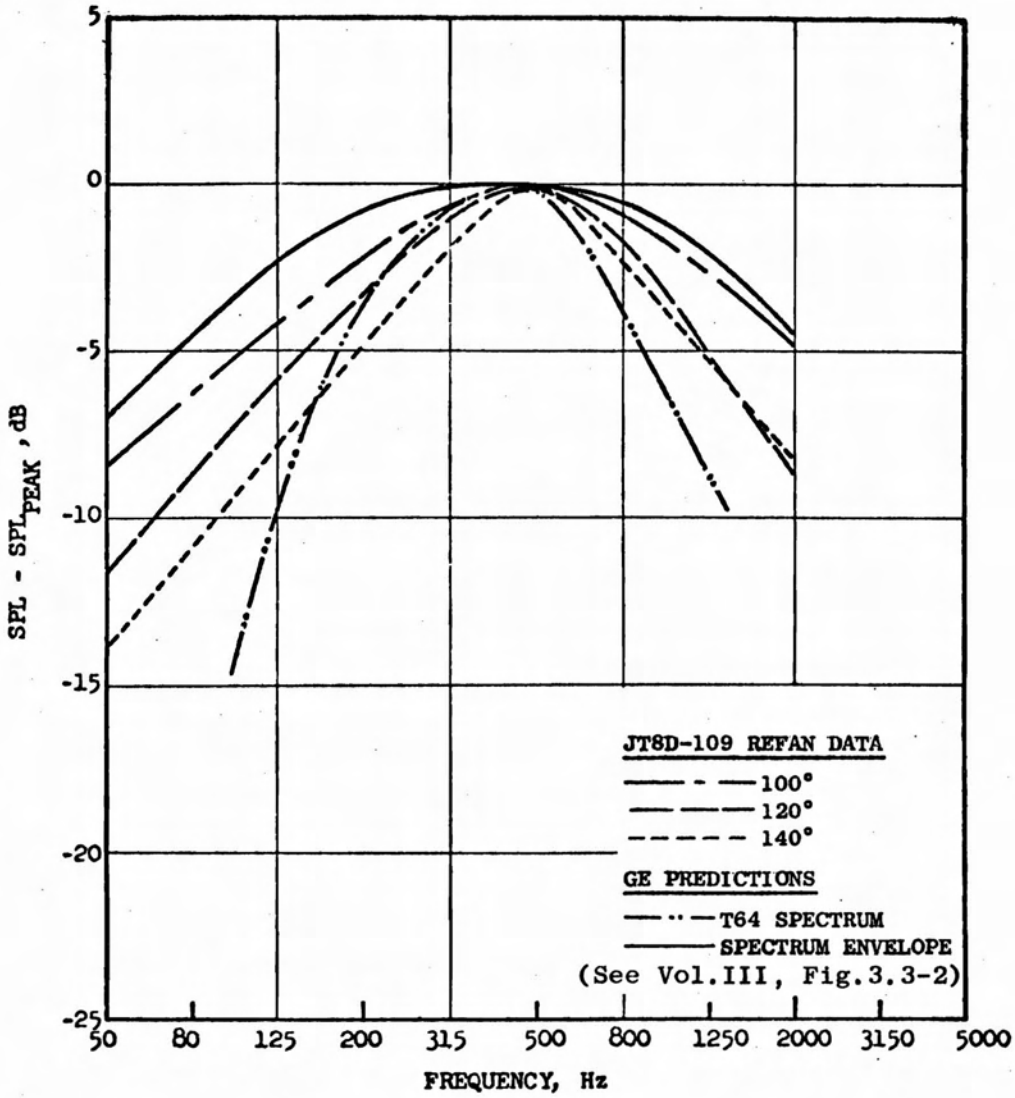

Figure 2-1. Comparison of Predicted and Measured Spectral Shapes of Low Frequency Core Noise.

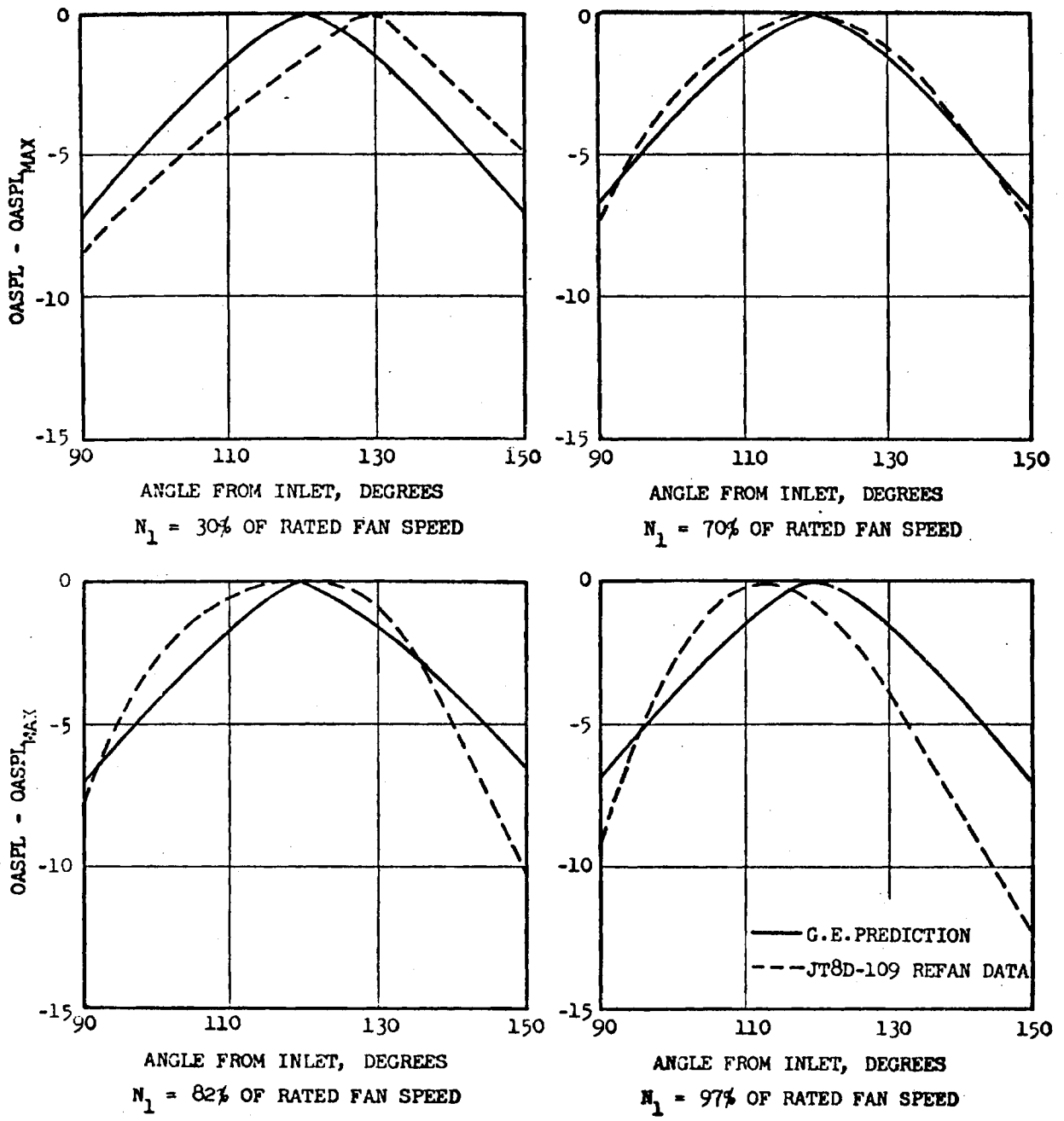

Figure 2-2. Comparison of Predicted and Measured Polar Directivities for the JT8D-109 Refan Engine.

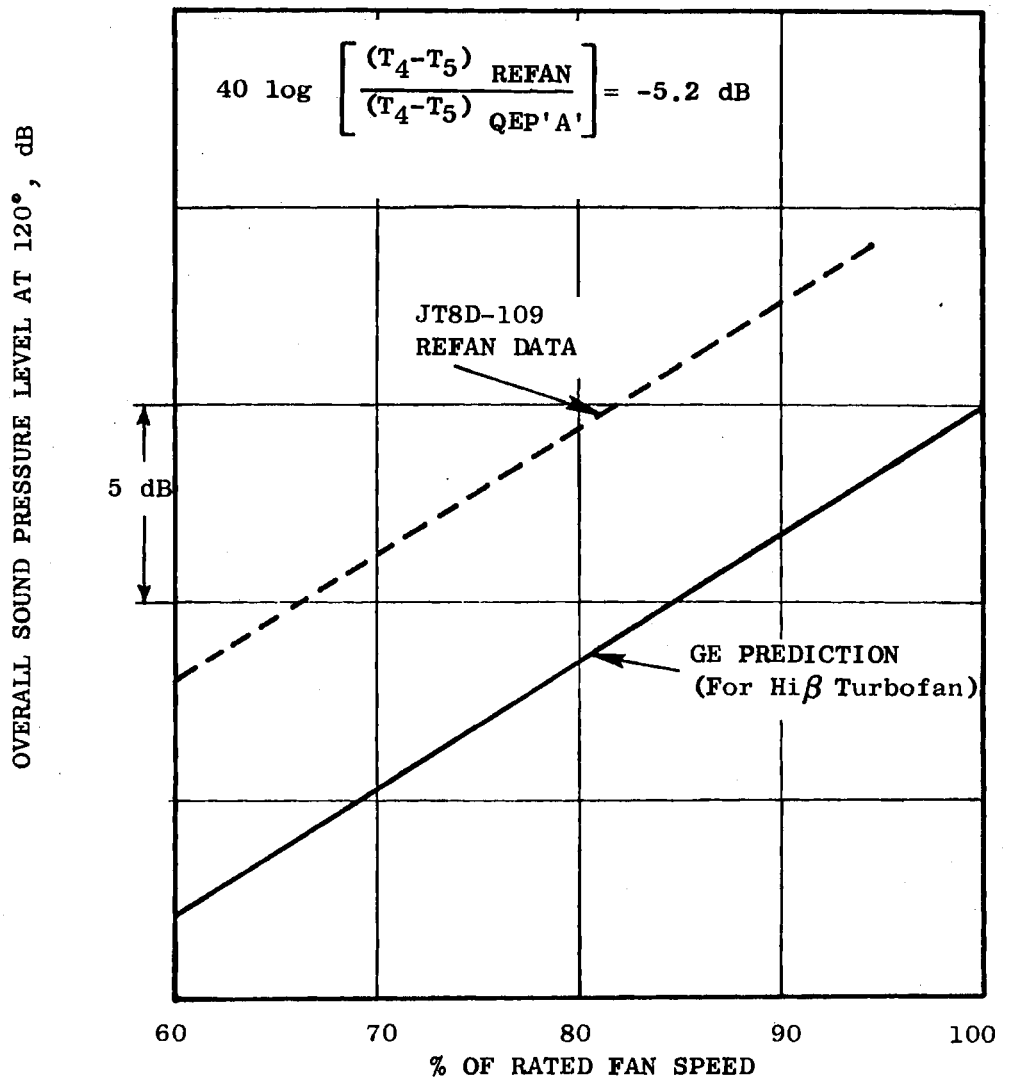

Figure 2-3. Comparison of Predicted and Measured Low Frequency Core Noise Levels for the NASA JT8D-109 Refan Engine.

however, is probably of greater significance. This involves the work extraction by the turbines. The transmission loss due to turbine blade row attenuation appears to be a function of the total temperature drop ($T_4 - T_5$) through the turbine stages and the three prediction lines for core noise OAPWL can be collapsed by normalizing the data through a 40 log ($T_4 - T_5$) factor - as is shown in Appendix A. It is interesting to note that at design point, ($T_4 - T_5$) for the refan engine was 830° R (461° K) while that for the typical high bypass turbofan engine used in the OAPWL correlation was 1120° R (622° K). The refan engine ($T_4 - T_5$) is more representative of the turboshaft engines used in the correlation. Based on these numbers, the refan engine data would lie within 1dB of the correlation when normalized by 40 log ($T_4 - T_5$) since this would account for 5.2 dB of the observed 6 dB difference between the refan data and the high bypass engine correlating line.

2.2 GARRETT TURBOSHAFT ENGINE

The low frequency core noise from turboshaft engines is relatively easy to evaluate, because fan noise does not exist, plus the jet noise is quite low. A turboshaft engine in the 840 shaft horse power (SHP) class was tested by Garrett-AiResearch Company (Reference 2). Various suppression devices were employed and their effects measured with farfield microphones located every 15 degrees on a 100 ft (30.48 m) arc. The configuration evaluated for core noise had a suppressed inlet and an untreated exhaust duct 9.3 inches (23.6 cm) long. The dynamometer which absorbed the shaft horsepower was sealed in an acoustical enclosure.

A comparison of a measured spectrum and the core noise prediction envelope can be seen in Figure 2-4. Below the first ground null, which occurs at 500 Hz, there appears to be the typical 6 dB pressure doubling due to ground reflections. At the higher frequencies, the continued nulls and reinforcement peaks which are caused by the ground effect can be seen. The levels of the spectra which were evaluated are not believed to be influenced by exhaust jet noise since the exhaust velocity did not exceed 250 ft/sec (76.2 m/sec). Therefore, below 1000 Hz, the spectra are dominated by core noise. Turbine noise is probably influencing the spectra above this frequency. Keeping the ground effects in mind, the prediction spectrum peaked at 400 Hz is seen to provide a good fit to the data.

The radiation directivity pattern for the peak frequency is plotted in Figure 2-5. The data scatter appears to be roughly what has been seen from the evaluation of other engine data. The peak level appears to occur at 135° from the inlet and is constant over the speed range tested. The prediction directivity, which peaks at 120°, still provides a reasonable approximation.

The overall power levels were determined from the turboshaft engine power level spectra. The prediction spectra envelope level and peak frequency were fitted to the power level spectra as in Figure 2-4. The overall level was determined as the peak level of the spectra plus 9.9 dB (where the 9.9 dB is the difference between the prediction spectral envelope's peak level and the

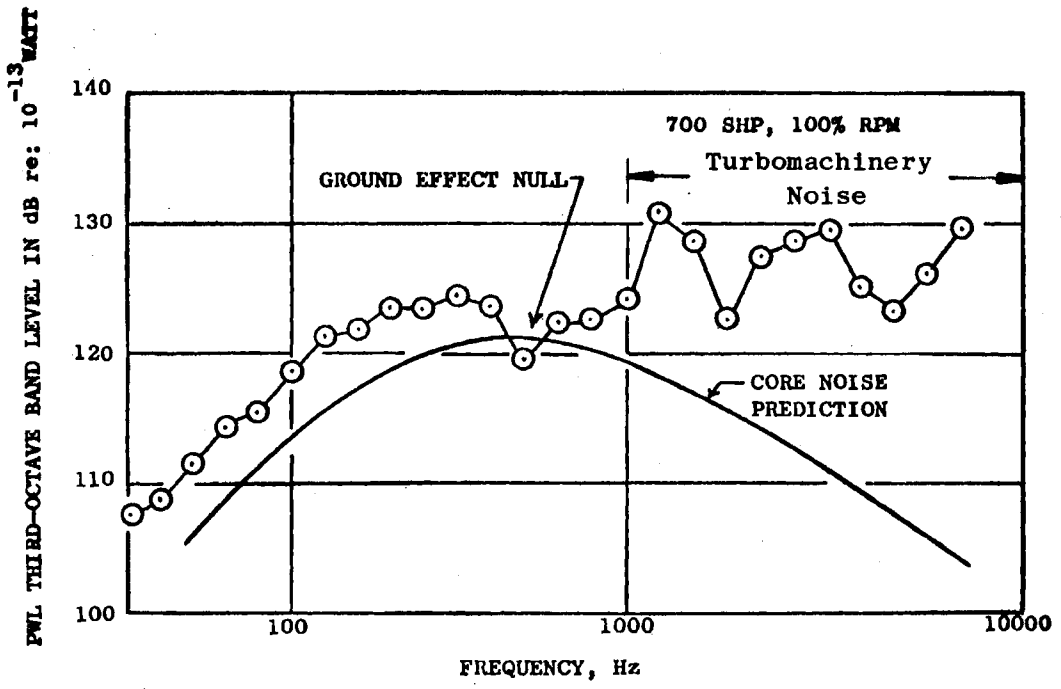

Figure 2-4. Spectral Shape Comparison of Turboshaft Data.

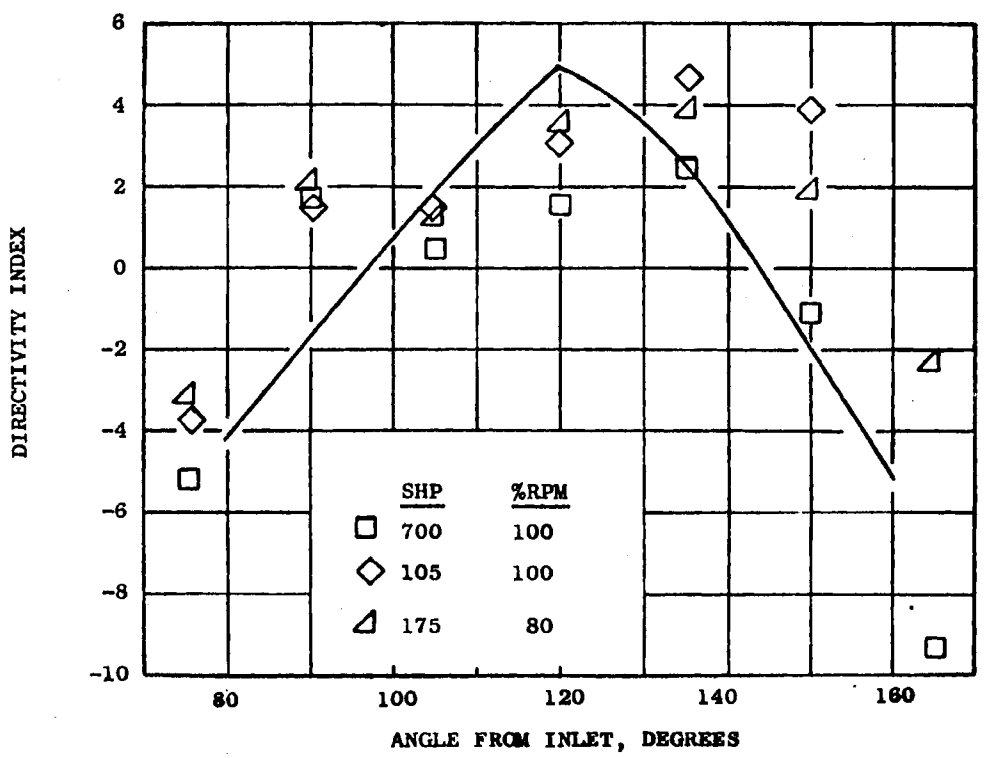

Figure 2-5. Turboshaft 400 Hz Directivity.

overall level for that spectral shape). The overall power levels determined by this method are plotted against the engine prediction parameter in Figure 2-6. The data can be seen to follow the same general trend as the turboshaft engine prediction line.

2.3 NASA TF34 ENGINE TEST

Comparison of NASA data (Figure 2-7) for configurations with varying amounts of treatment generally indicate significant core noise contribution to the farfield levels for speeds below 5100 rpm. The low frequency noise suppression shown in the spectra is due to a fairly short (12-inch) and deep (4-inch) bulk absorber used in the core nozzle along with the usual high frequency turbine treatment.

The low frequency suppression cannot be seen at the higher power settings, indicating jet noise domination of the spectrum. These observations were verified by plotting the directivities for the affected frequencies.

Earlier in the Core Engine Noise Program, core noise estimates for the TF34 were derived from General Electric data and spotted on the OAPWL prediction curve. However, these data included considerable undulations (possibly ground reflection) in the spectra and hence there was some doubt whether:

a. core noise was present in the farfield spectra (this question has been addressed above), and

b. the valleys and peaks in the spectra could be attributed entirely to ground reflections and, therefore, the freefield spectra defined by simply faring in a smooth line.

General Electric data are compared with the NASA ground microphone spectra in Figure 2-8. A one-to-one comparison is impossible since the General Electric data are for separate flow configurations (fan exhaust upstream of core exhaust) while those from NASA are for a confluent flow configuration. It is clear however, that the undulations in the General Electric spectra (below 1000 Hz) do result from ground reflections. The agreement between the General Electric and NASA levels indicate that the early General Electric estimates of TF34 core noise were fairly good.

2.4 BOEING DATA

The Boeing Company has provided data from six turbofan engines in a comparison with the prediction. The overall sound pressure levels at the 120° angle on a 200 foot (60.96m) sideline were plotted (Figure 2-9) against the prediction parameter. It was observed that the high bypass ratio turbofan engine data agreed very well with the turbofan prediction line. However, the low bypass turbofan fell close to the turboshaft line similar to the results (Figure 2-3) for the Refan.

Note that the data in Figure 2-9 extend to power settings beyond the original correlation.

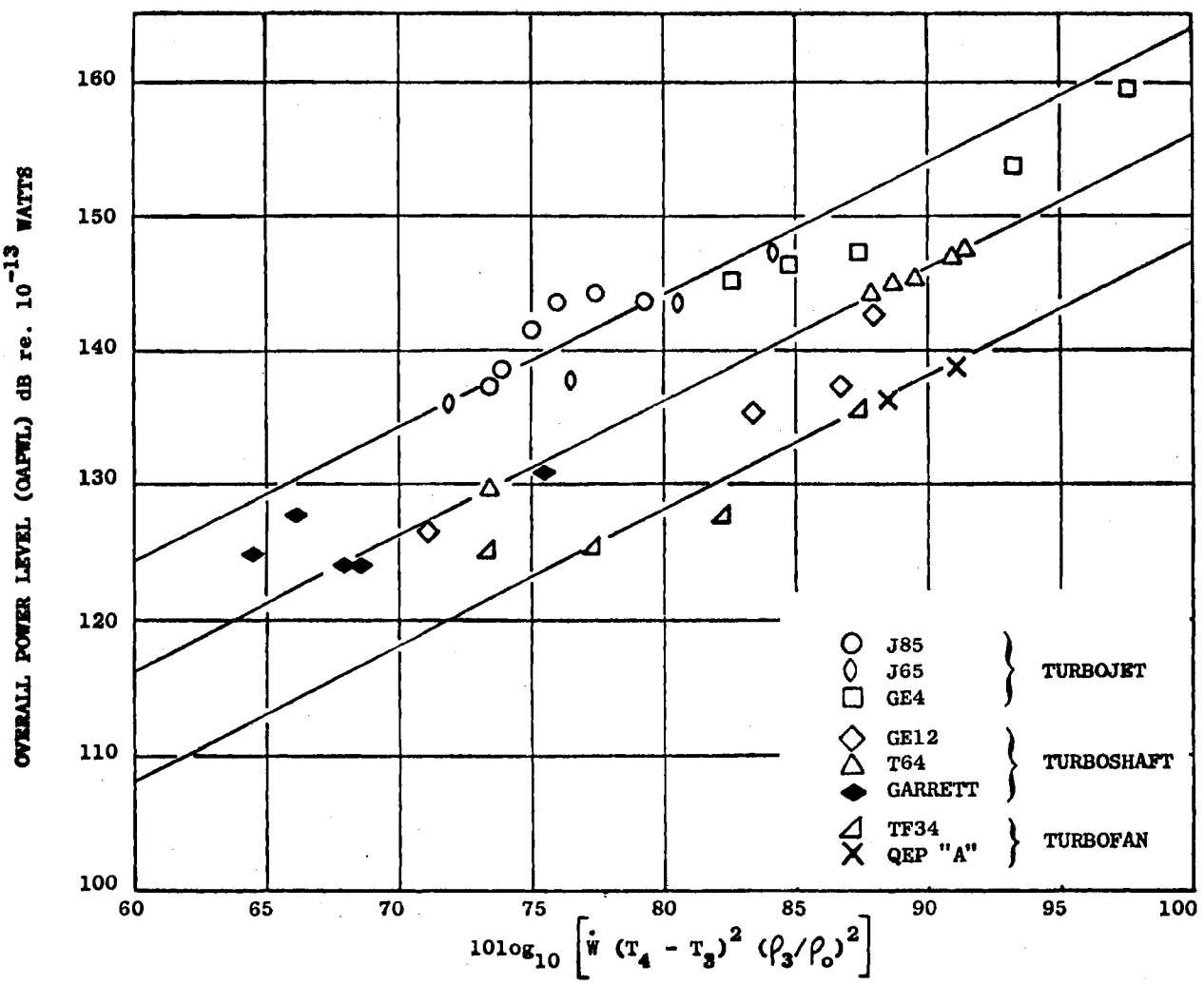

Figure 2-6. Comparison of Turboshaft Power Levels To The Prediction Parameter.

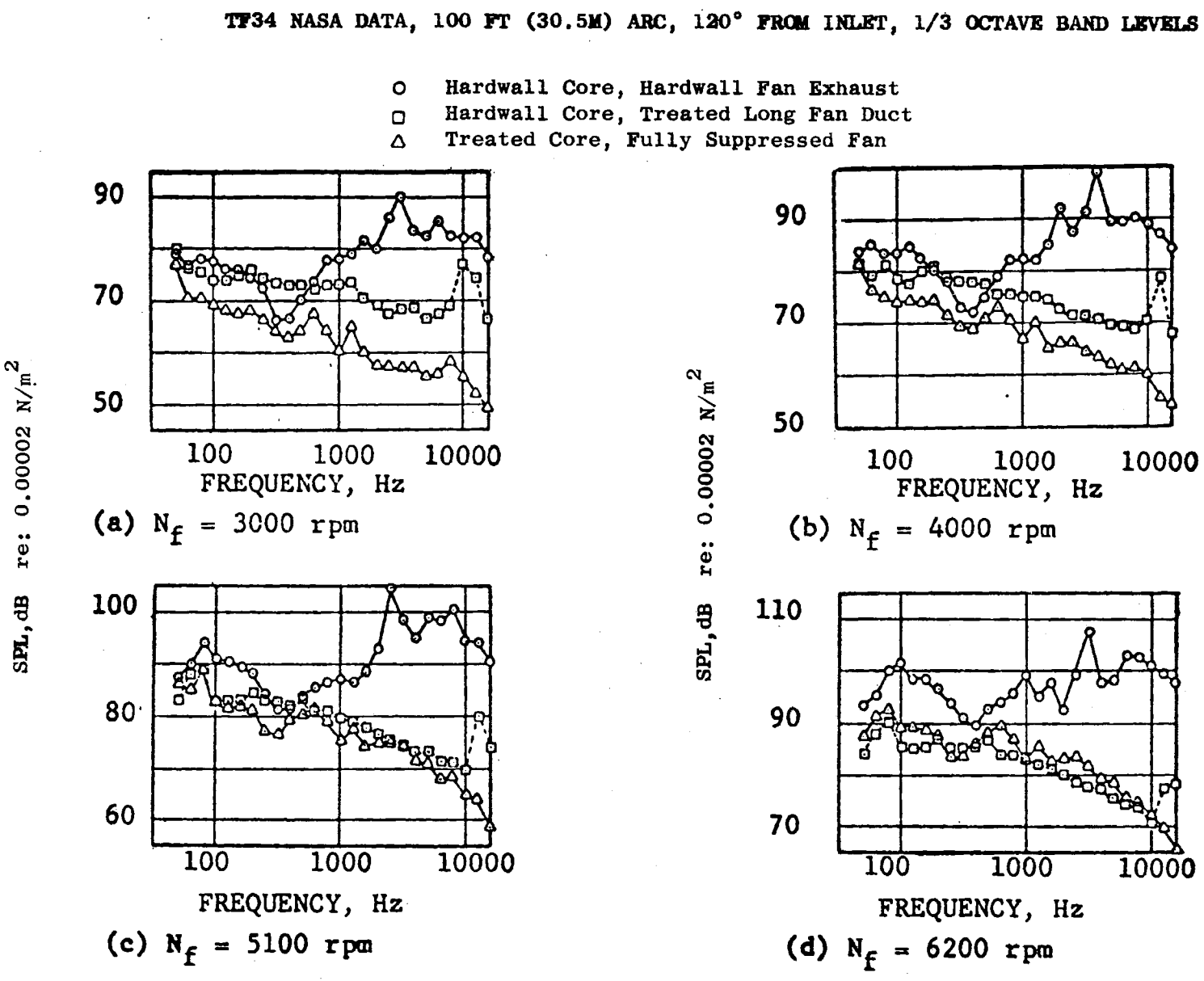

Figure 2-7. TF34 Spectral Comparison Using Engine Center-Line Microphones.

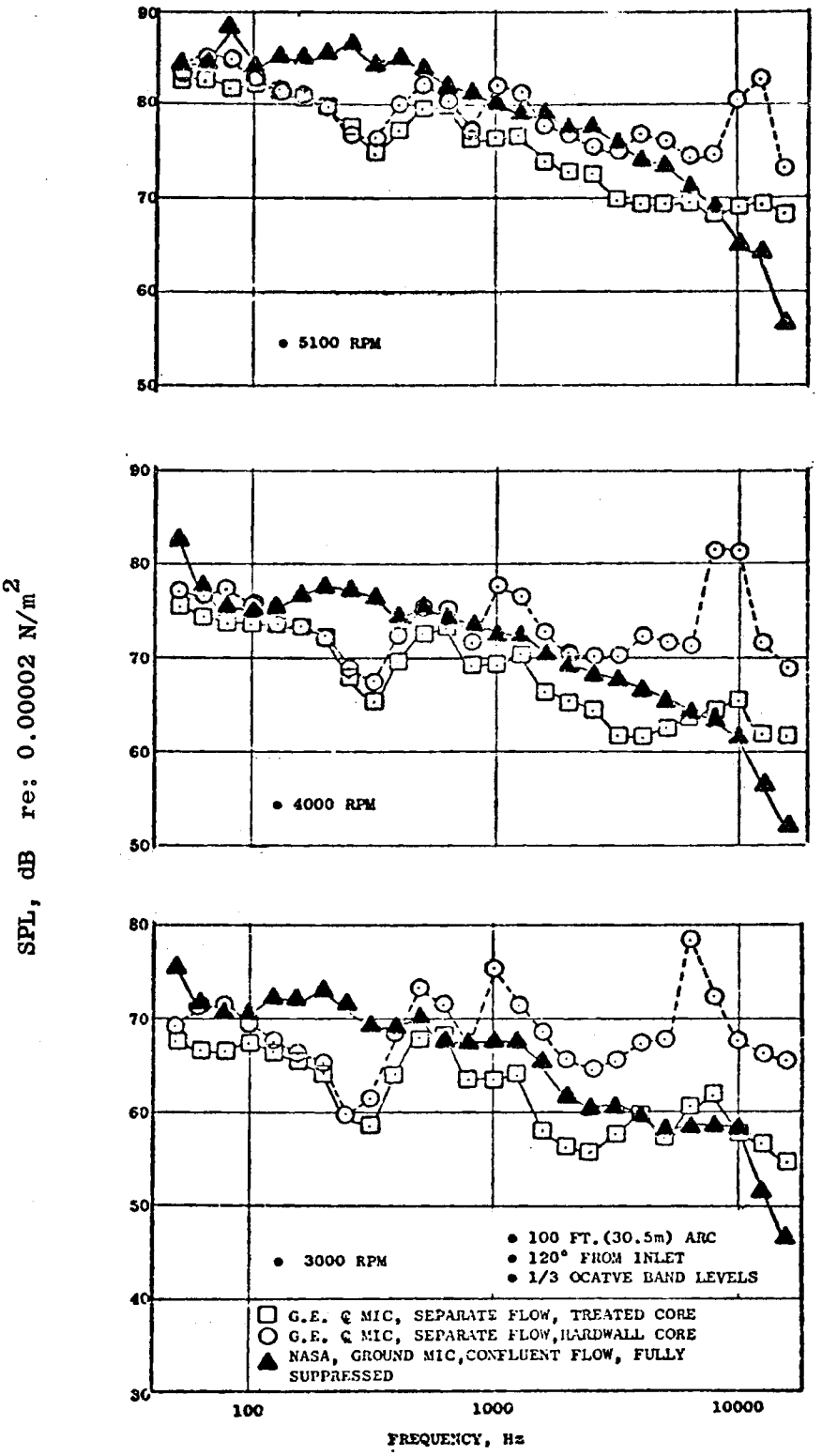

Figure 2-8. Comparison of GE and NASA TF34 Engine Data.

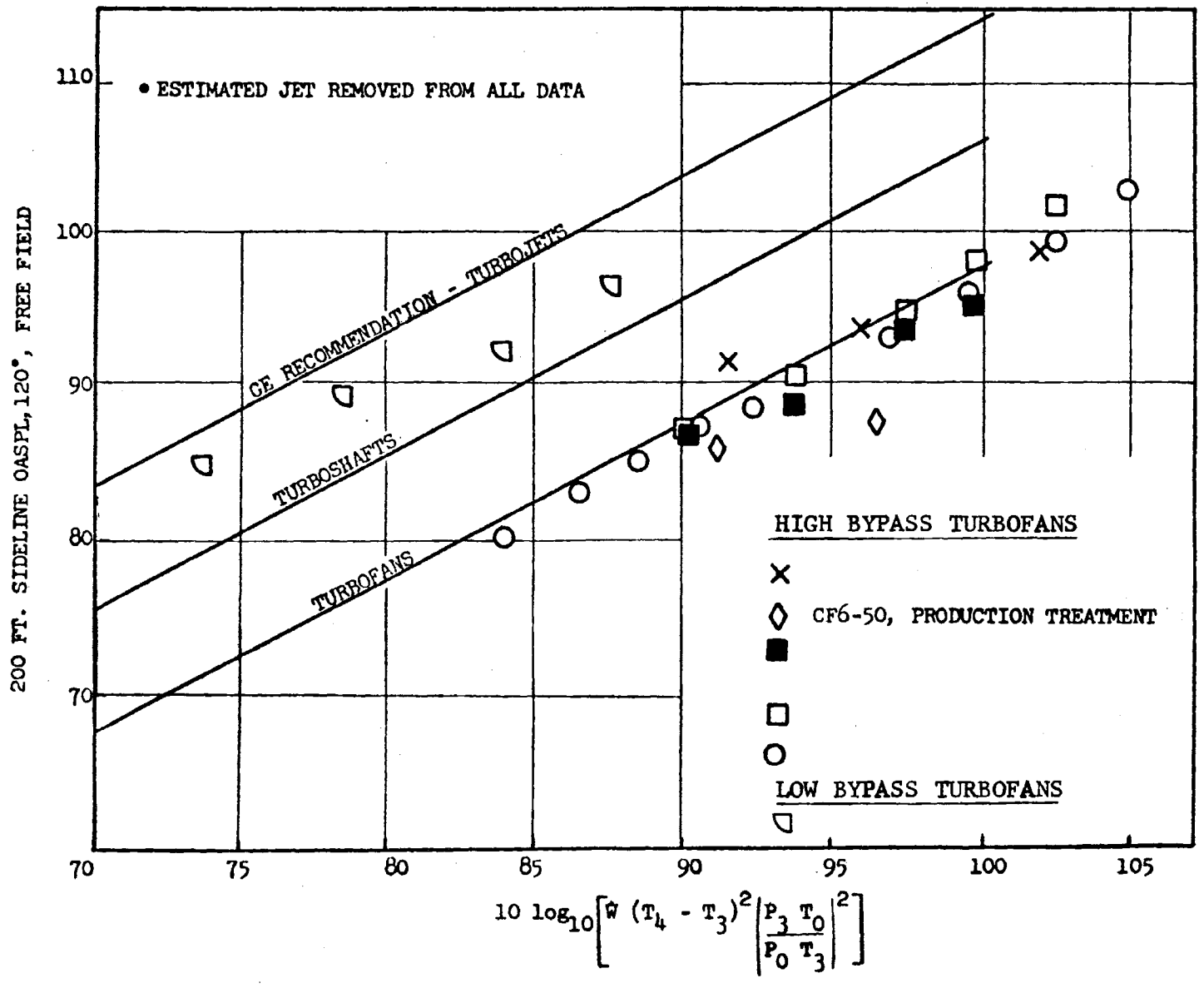

Figure 2-9. Comparison of Boeing Data with GE Procedure.

SECTION 3.0

ENGINE HIGH POWER SETTING EVALUATION

Examination of acoustic data from turbojets and turbofans at high power settings revealed that in most cases jet noise contaminated or overshadowed the core noise in the aft quadrant. In order to provide additional high power setting data an investigative technique consisting of studying the exponent of the exhaust velocity for each frequency at each angle along with the effects of acoustic treatment on the contaminating noise sources was used.

Acoustic data was evaluated for discernible core noise at high power settings on the T64, GE12, Quiet Engines "A" and "C", TF34, CF6, J65, J79, J85 and GE4.

There was no problem with jet or fan noise contamination for the turboshaft engines (T64, GE12). Data encompassing the entire operating range is spotted on the prediction line. The Garrett data also included high power settings. The examination of turbofan engine data revealed that Engine "A" data provided discernible core noise levels over the entire operating range of the engine. The data from the other engines mentioned above did not yield any significant or consistent indications of core noise at high power settings.

3.1 THE SPECTRUM LEVEL

The primary problem of evaluating core noise at the higher power settings is the contaminating influence of other noise sources, mainly the fan and the jet. There are two methods that can be used to evaluate the relative effects of these other noise sources. The effect of fan noise can be evaluated by comparing the spectral data from an unsuppressed fan to a fully suppressed fan configuration at the angle where core noise is expected to peak, namely 120° from the engine inlet (see Section 3, Volume III). When the levels of the two spectrums converge it can be reasonably assumed that the fan has little or no effect on the spectrum.

The presence of jet noise can be determined by examining the sound pressure levels for the individual one-third octave frequency bands and plotting them against the core exhaust velocity over the operating range of the engine. When the slope of the plot indicates an exhaust velocity to the sixth power or higher relationship, it can be assumed that jet noise is dominating the spectrum. However, when the slope of the data indicates an exhaust velocity to the fourth power dependency, it can be assumed that some other source dominates. Hence, the one-third octave band levels, which could not be identified as either fan noise or jet noise and which followed a core exhaust velocity to the fourth power, are indicative of core noise.

Data from Engine "A" of the NASA Quiet Engine Program provide a good set of data for evaluation of core noise at the higher power setting. Figure 3-1 shows a low power setting spectrum at 120° from the inlet. The region of fan noise dominance can be seen beginning at 1250 Hz and continues to 10,000 Hz. On the very low frequency end, jet noise can be seen to dominate. The prediction for coannular jet noise is plotted over the measured data. The remaining portion of the spectrum, between 400 and 1000 Hz, has the core noise prediction spectrum drawn in. The influence of jet noise at any particular one third octave band is evaluated from the exponent of the exhaust velocity (Figure 3-2). At 315 Hz a line representing the exhaust velocity raised to the sixth power has been drawn through the data. The close fit of the data at this frequency indicates that jet noise is dominating over the whole engine speed range with the exception of the lowest speed point. This lowest point diverges in a direction which would indicate a velocity to the fourth power, or the presence of core noise. This same trend is observed at 400 Hz. At 500 Hz however, there is a divergence from the velocity to the sixth power which now occurs at a higher power setting. At this frequency the lowest three points appear to be core noise and the upper 3 points appear to be jet noise dominated. The next three frequencies, (630, 800 and 1000 Hz) clearly follow the exhaust velocity to the fourth power relationship over the entire engine speed range.

The frequency range of core noise dominance as a function of engine power-level was evaluated from the spectra. Figure 3-3 shows three engine spectra, each with the component sources which generate the spectrum indicated. The level of the core noise can be determined by fitting the core noise prediction spectrum to the engine data. Based on the peak level of this spectrum and the core noise prediction directivity the core noise power levels can be obtained over the engine's entire speed range. The power levels calculated by this method are plotted against the core noise prediction parameter in Figure 3-4. As can be seen, the level follows the prediction line for turbofan engines very well.

These data verify that the core noise prediction parameter is valid over the whole operating range of an engine.

3.2 SPECTRAL SHAPE AT HIGH POWER SETTINGS

At the lower power settings, the core noise prediction spectrum fits the measured Engine "A" data for 6 one-third octave bands (Figure 3-3). When the engine speed is increased to 95% fan speed the slope of the jet noise spectrum approaches the slope of the core noise spectrum; however the core noise spectrum still maintains a good fit over 5 one-third octave bands. There is no indication that the core noise spectral shape differs appreciably from the prediction spectrum over the engine operating range.

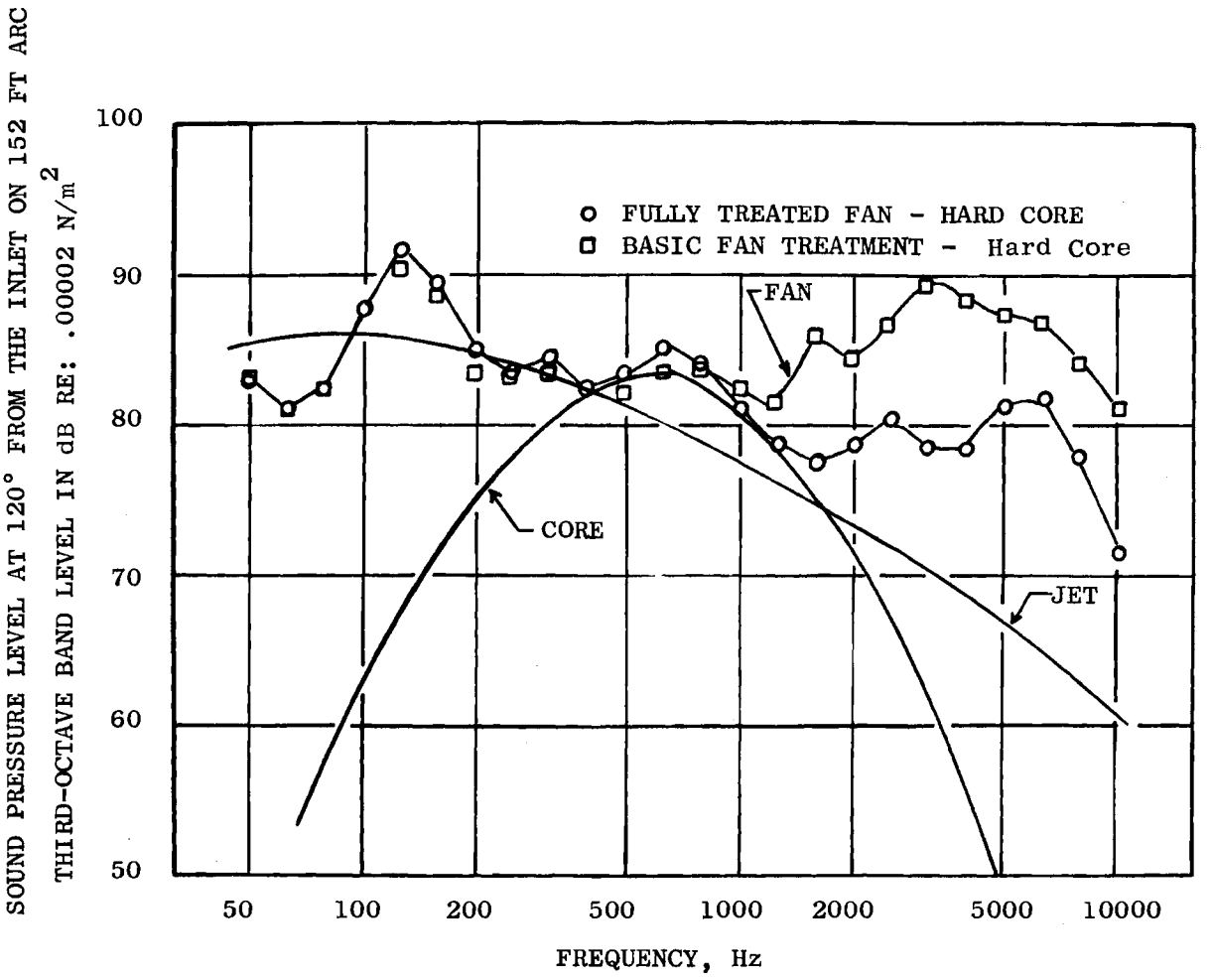

Figure 3-1. Engine "A" Quiet Engine Program at 70% Fan Speed.

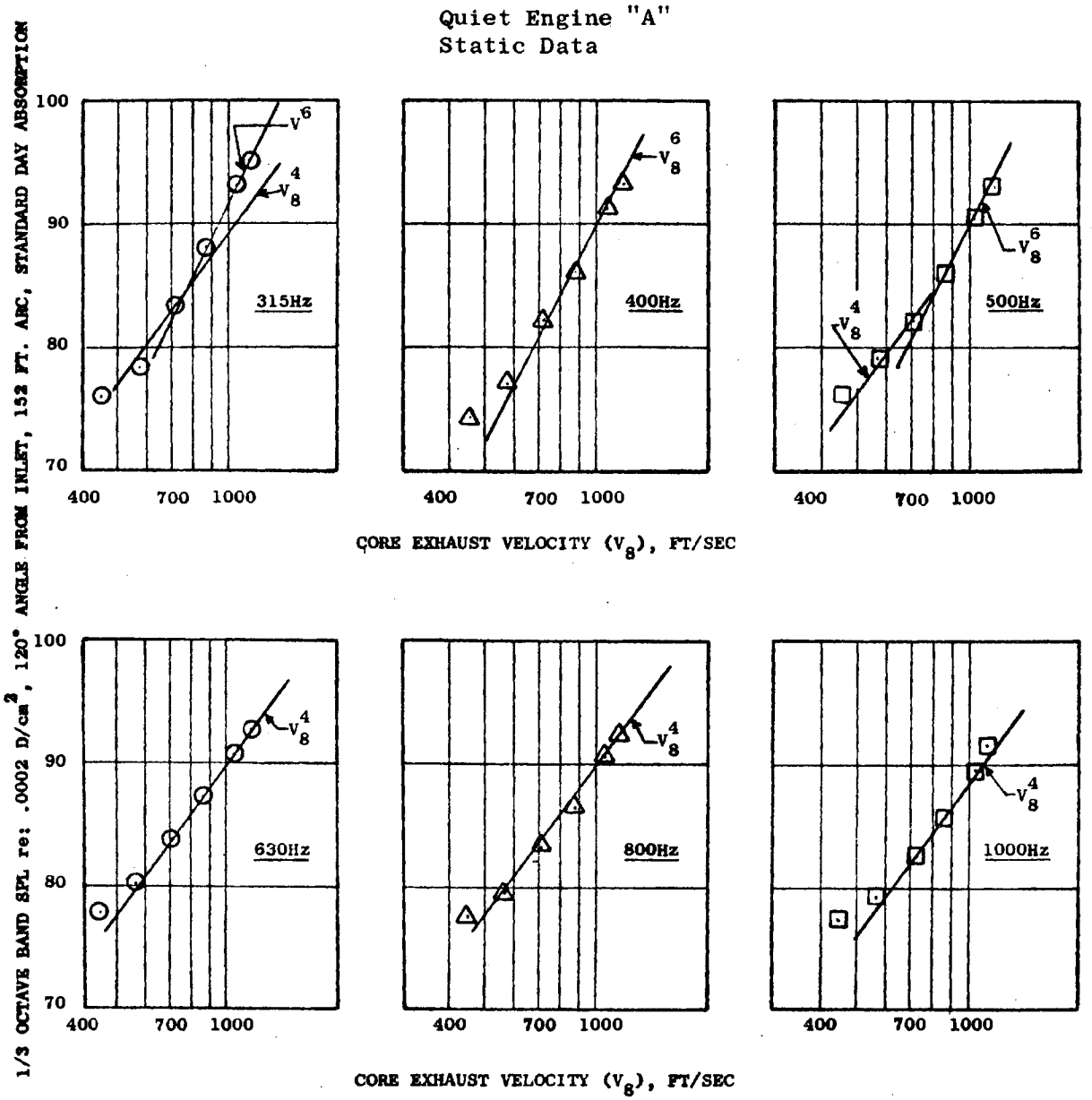

Figure 3-2. The Limit of Jet Noise Determined by the Exponent of the Exhaust Velocity.

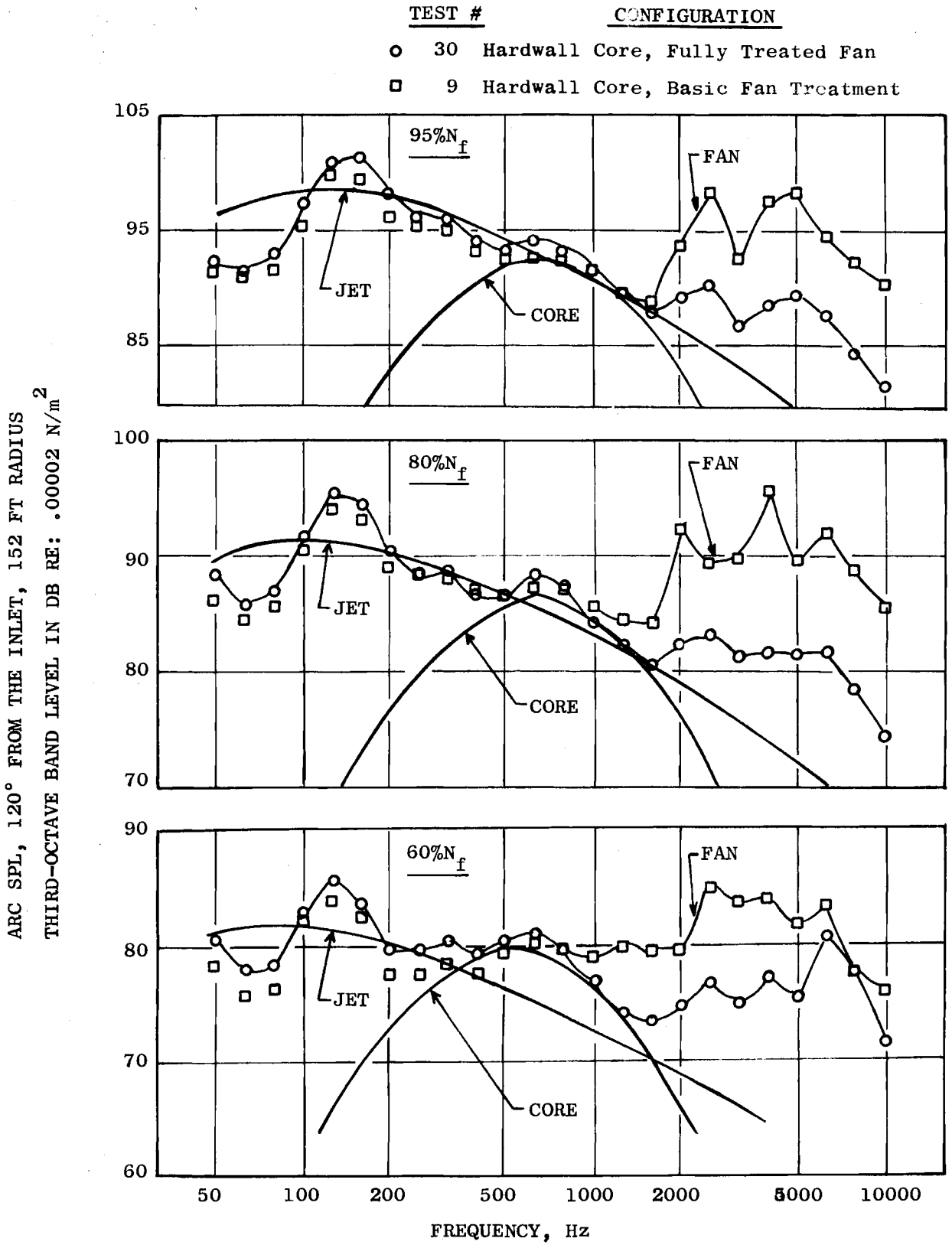

Figure 3-3. Comparison of QEP "A" Engine Spectrum.

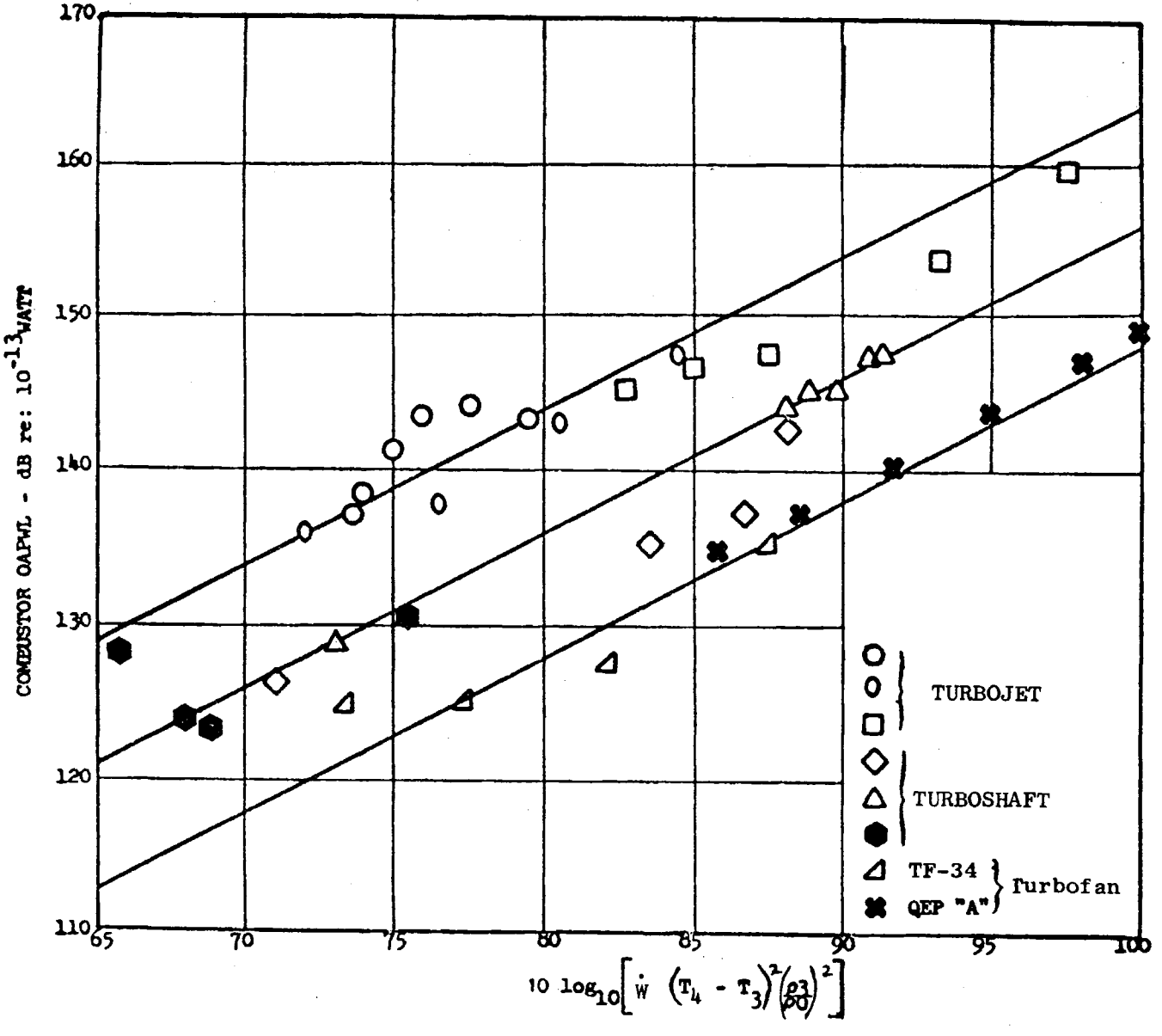

Figure 3-4. Engine "A" Core Noise Levels for Power Settings from Idle to Takeoff Speeds.

3.3 ENGINE HIGH POWER SETTING DIRECTIVITY

At the higher power settings it was found that for angles greater than 120° the directivity pattern followed the jet noise prediction. At fan speeds higher than approximately 70%, jet noise has a significant influence on the directivity. In this case it is assumed that the core noise directivity does not change at the higher power levels.

As was noted earlier, the turboshaft data were found to include significant core noise over the entire operating range, as were those from Engine "A". The data from the other engines were found to be controlled by either jet or fan noise.

The Boeing data (Figure 2-9) also extends to high power settings and thus provide additional verification of the prediction line.

SECTION 4.0

ADDITIONAL COMPONENT DATA

4.1 COMPONENT COMBUSTOR SPECTRA

Component combustor tests were preformed at atmospheric pressure under the original portion of this program. The results are reported in Volume II (Section 3). The acoustic data were originally acquired with 16 ft (4.88 m) high microphones on the 40 ft (12.19 m) radius arc, however, ground reflections were found to create nulls and peaks in the low frequency region of the spectra. A spectral correction for these ground effects was obtained from a comparative examination of data taken with microphones at the 16 ft (4.88 m) and 2 ft (0.61 m) height. The two foot microphone height moves the first null of the ground reflection to a frequency of about 2000 Hz and out of the range of interest. These corrections were applied to the original data taken at the higher microphone height. The resulting spectra are plotted in Figures 4-1 and 4-2 for the Advanced Technology (AT) and CF6 combustors respectively. For comparison purposes the core noise prediction spectrum shape is shown for one temperature setting. The prediction spectrum shape agrees with the shape of the data, however the frequency at which the peak occurs is 200 Hz. This is two one-third octave bands lower than what would be expected from the current engine core noise prediction procedure. The difference may be due to the downstream turbine blade rows and the nozzle end impedance encountered in engines. Cross sectional schematics of a turbofan engine, an atmospheric pressure component combustor test rig, and a high pressure component combustor test configuration are shown in Figure 4-3.

Noise measurements of component combustors operating at high inlet temperatures and pressures were taken by GE under the Experimental Clean Combustor Program (Contract No. NAS3-18551). This program involved testing three design philosophies of low emission full scale annular combustors, the Swirl-Can, Radial/Axial, and Double Annular. The combustors were tested in a high pressure component test rig. Acoustic probes measured the levels immediately downstream of the combustor. Representative sound pressure level spectra can be seen in Figure 4-4. Simulated approach and takeoff combustor inlet conditions are shown. The spectral envelope peaks at 500 Hz and is seen to be in good agreement with the measured spectra for all the configurations at approach power conditions. The T64 spectrum, which falls off somewhat rapidly above 1000 Hz, is also shown. At the takeoff (inlet) condition, however, some of the configuration's peak levels appear to shift to a higher frequency. The spectral envelope is peaked at 800 Hz and fits the Double Annular and the 90-Swirl-Can spectra. The Radial/Axial combustor shows higher levels at the higher frequencies, but can not be considered a typical annular combustor. This configuration employed afterburner type flameholders which are believed to be responsible for the broader spectral shape. Again, the end termination was somewhat different from that for engines, and this may involve a spectral re-ordering due to frequency dependent attenuation and radiation.

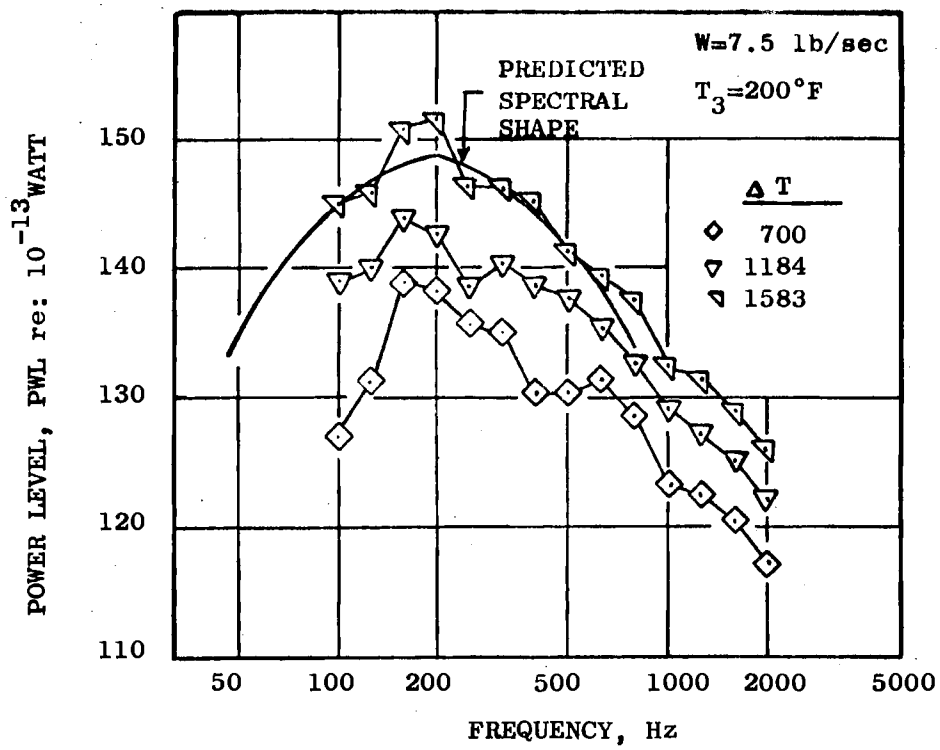

FIGURE 4-1 POWER LEVEL (CORRECTED FROM 16 FOOT HIGH TO 2 FOOT HIGH MICROPHONES), F101 COMPONENT COMBUSTOR

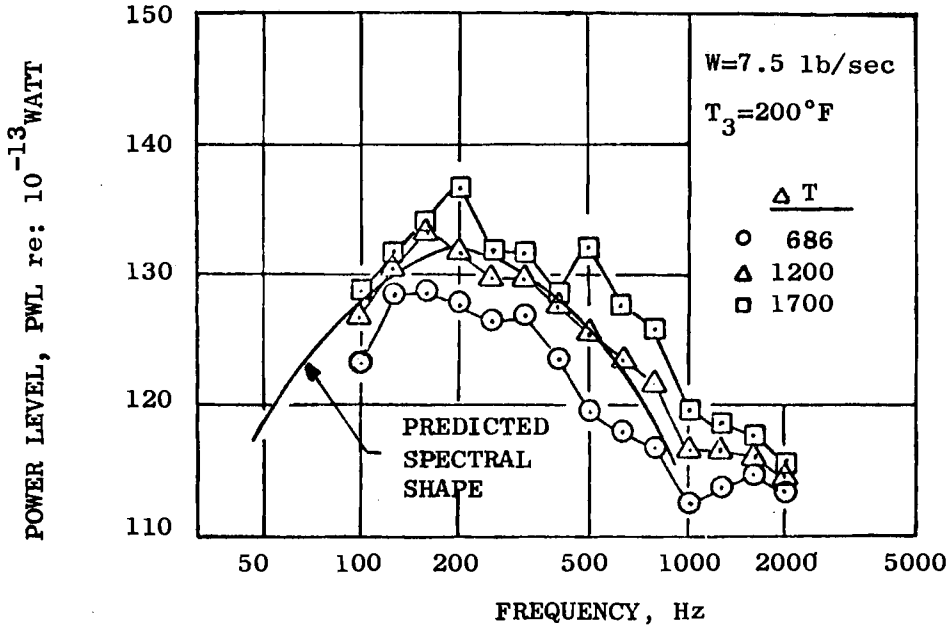

Figure 4-2. Power Level (Corrected from 16 foot High to 2 foot High Microphones) CF6 Component Combustor.

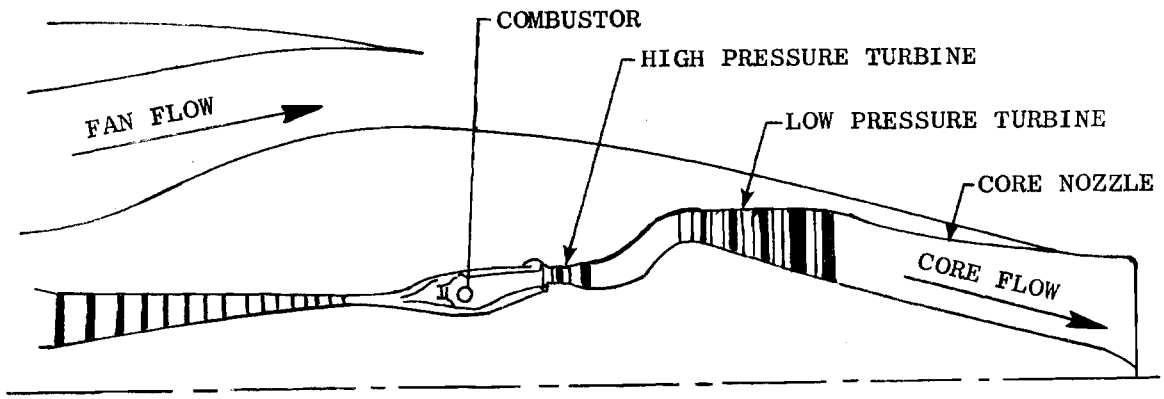

TURBO-FAN ENGINE FLOW PATH

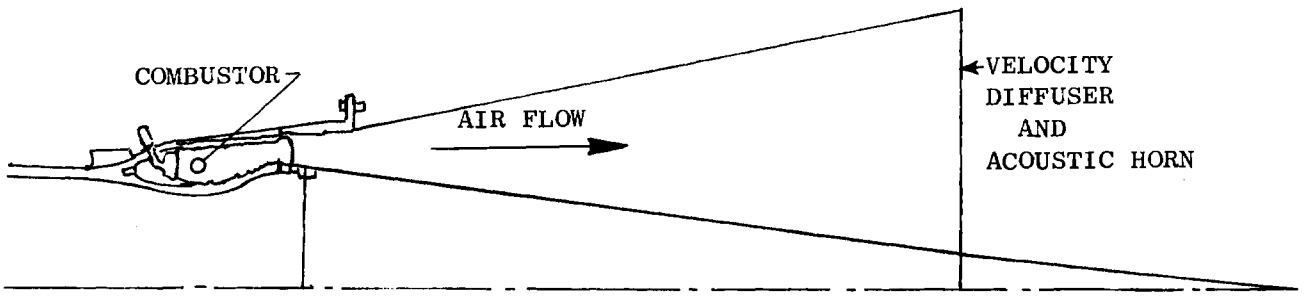

ATMOSPHERIC PRESSURE COMPONENT COMBUSTOR TEST RIG

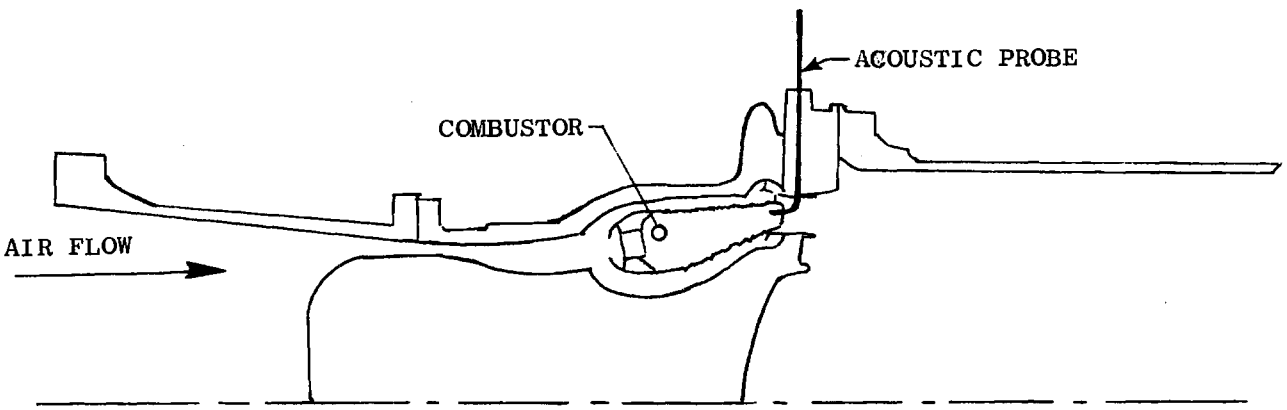

HIGH PRESSURE COMPONENT COMBUSTOR TEST RIG

Figure 4-3. Comparison of an Engine to Component Test Configuration.

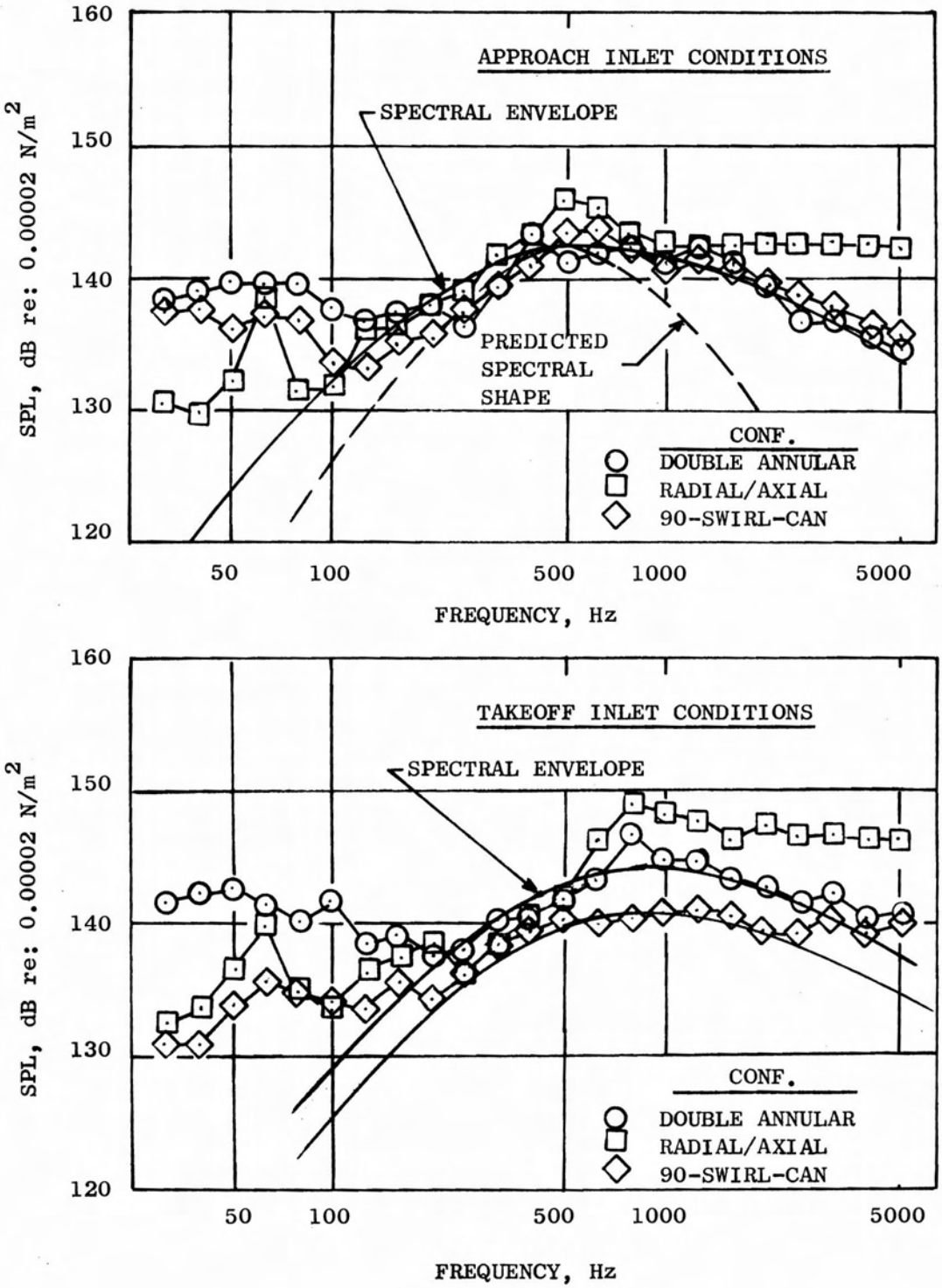

Figure 4-4. Comparison of Six Combustors with the Downstream Probe at a Constant Fuel-Air Ratio of 0.0245.

The higher pressure combustor noise tests appear to fit the broader spectral envelope, while the engine data in general tend to follow the T64 (narrower) spectrum. The difference may be attributed to the effect of the turbine blade rows downstream of the combustor in the case of engines.

4.2 COMPONENT COMBUSTOR POWER LEVEL

The noise levels of the component combustors can be compared on a power level basis. The CF6 and AT combustor power levels were calculated from far-field arc data. Their overall levels were arrived at by logarithmically summing the one-third octave band power levels over the frequency range of 100 to 2000 Hz. The high pressure combustor data were summed over the 31.5 to 5000 Hz frequency range and the power level was calculated based on the local temperature, pressure, Mach number and cross section annulus area:

$$PWL = SPL + 10Log_{10}(A) + 10Log_{10}\left[\frac{P_o}{P}\sqrt{\frac{T}{T_o}}\right] + 10Log_{10}\left[(1+M_N)^2\right] + K$$

where A is the annulus area (square meters) at the probe's sensing holes, P and T are the local pressure (atmospheres) and temperature (°K) where the subscripts indicate standard day reference levels and M_N is the Mach number of the flow past the probe. The constant K is the sum of the SPL and PWL reference levels and the standard day characteristic impedance of the medium. It should be noted that there is no coefficient in front of the Mach number. A coefficient may be used if it is assumed the acoustic waves strike the probe at random incidence angles. The wavelength of the sound being considered is much larger than the passage height dimension, therefore a plane wave assumption can be made which makes the coefficient unnecessary. The standard day reference temperature and pressure are 288° K and one atmosphere. The constant K is 9.9 dB.

These overall power levels are compared by plotting them against the engine prediction parameter (Figure 4-5). The major portion of the component data fall above the turbojet prediction line.

The grouping of the 3 classes of engines and the relationship of the component noise power levels to the engine data strongly suggests an attenuation mechanism for combustor noise along the propagation path through the turbine stages and exhaust duct.

4.3 TURBINE BLADE ROW ATTENUATION

The attenuation of low frequency noise through a turbine stage has been analytically predicted by K. Bekofske (Reference 3). His study is based on an actuator disk model. An actuator disk is a cascade model with infinitesimal chord length and blade spacing. Since combustor low frequency acoustic energy in the high temperature environment has characteristic wavelengths that are large when compared to both the chord and transverse spacing of a blade

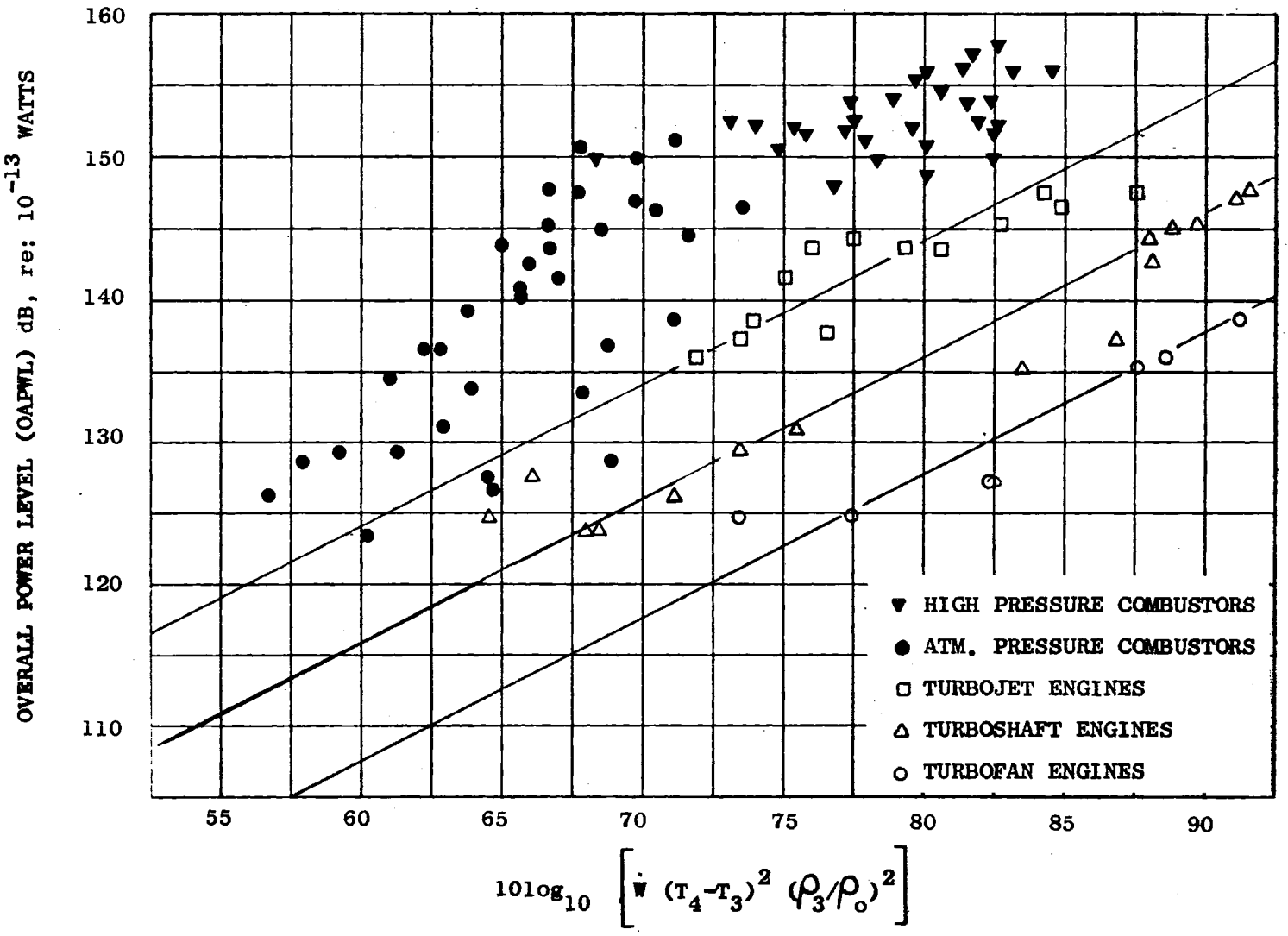

Figure 4-5. Component Combustor Power Level Vs. Prediction Parameter.

row, the use of the actuator disk model is justified. In this analysis, the relative Mach number at both the inlet and discharge side of either the nozzle or bucket has been assumed to be subsonic.

The stage attenuation is the difference between the initial wave and the wave amplitude transmitted through the stage. This difference is determined by a reflection coefficient. An infinite duct is assumed upstream of the blade row such that the reflected ray continues propagating upstream and is completely removed from the system. The calculation of this reflection coefficient takes into effect the changes in Mach number and the flow turning angle. The stage attenuation can be calculated as a function of the initial wave incidence angle. It is assumed that the initial wave incidence angle on each stage is close to zero degrees, (which represents a plane wave striking the stage normally, Figure 4-6). In actuality it is expected that there is some distribution of the incidence wave as a function of angle, with the highest probability at zero degrees.

The input to a computer program based on this analysis (listed in Appendix B) consists of the axial velocity, absolute flow angle, static pressure and total temperature at three locations in any given stage: upstream of the nozzle, between the nozzle and bucket, and downstream of the bucket. The aerodynamic parameters of each stage of both the high and low pressure turbines of a typical high bypass turbofan engine for a takeoff condition were input to this computer program. Figures 4-7 and 4-8 show the first stage of the high pressure turbine and the last stage of the low pressure turbine for a typical high bypass ratio engine. Both figures show an angle where the attenuation sharply increases. Incident waves whose angles are larger than these angles will be cut off and theoretically no portion of their acoustic energy will be transmitted.

Table 4-1 lists the stage total attenuation at zero degrees for each stage and the total attenuation for the seven turbine stages. A total of 38.9 dB is predicted for this takeoff condition. From the examination of the low pressure turbine (Table 4-2) attenuation as a function of engine speed, it was found that the attenuation does not appreciably change with power setting. A comparison of the component and turbofan correlating line indicates that the analysis somewhat over predicts the attenuation occuring in transmission through the blade rows. This over prediction of the attenuation might be attributed to: (1) the assumption that the energy reflected at a blade row is completely removed from the system. In reality, the reflected wave can propagate upstream to the next blade row and part of this may be reflected back downstream, effectively reducing the attenuation and (2) conditions in an engine which deviate from the assumed mean flow between stages. In particular, the incidence angle may vary from zero. The trend in the measured data and the analytic prediction nevertheless, both indicate significant attenuation of noise propagating through the turbine. Further development of the blade row attenuation prediction technique is required. This work has been initiated under Contract NAS3-19435.

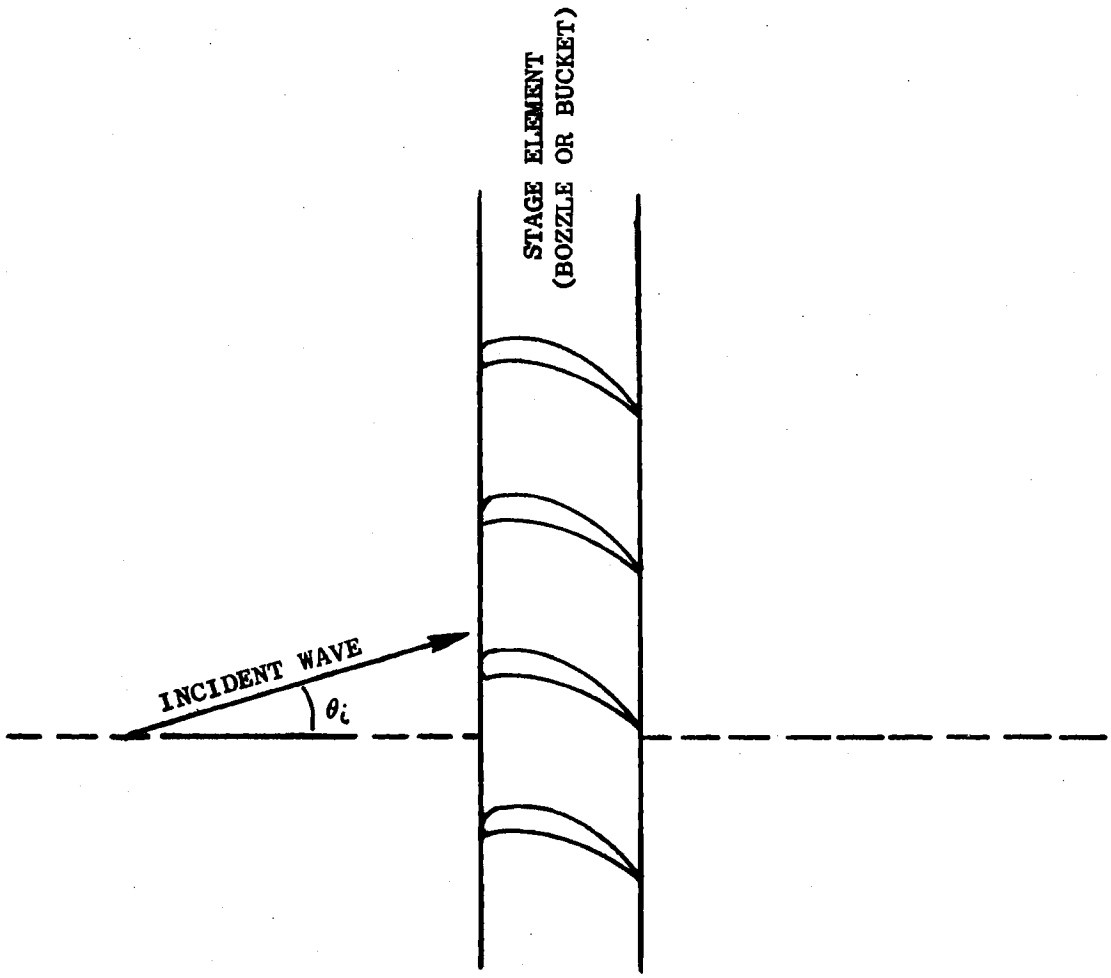

Figure 4-6. Geometry of Incident Wave on a Stage Element.

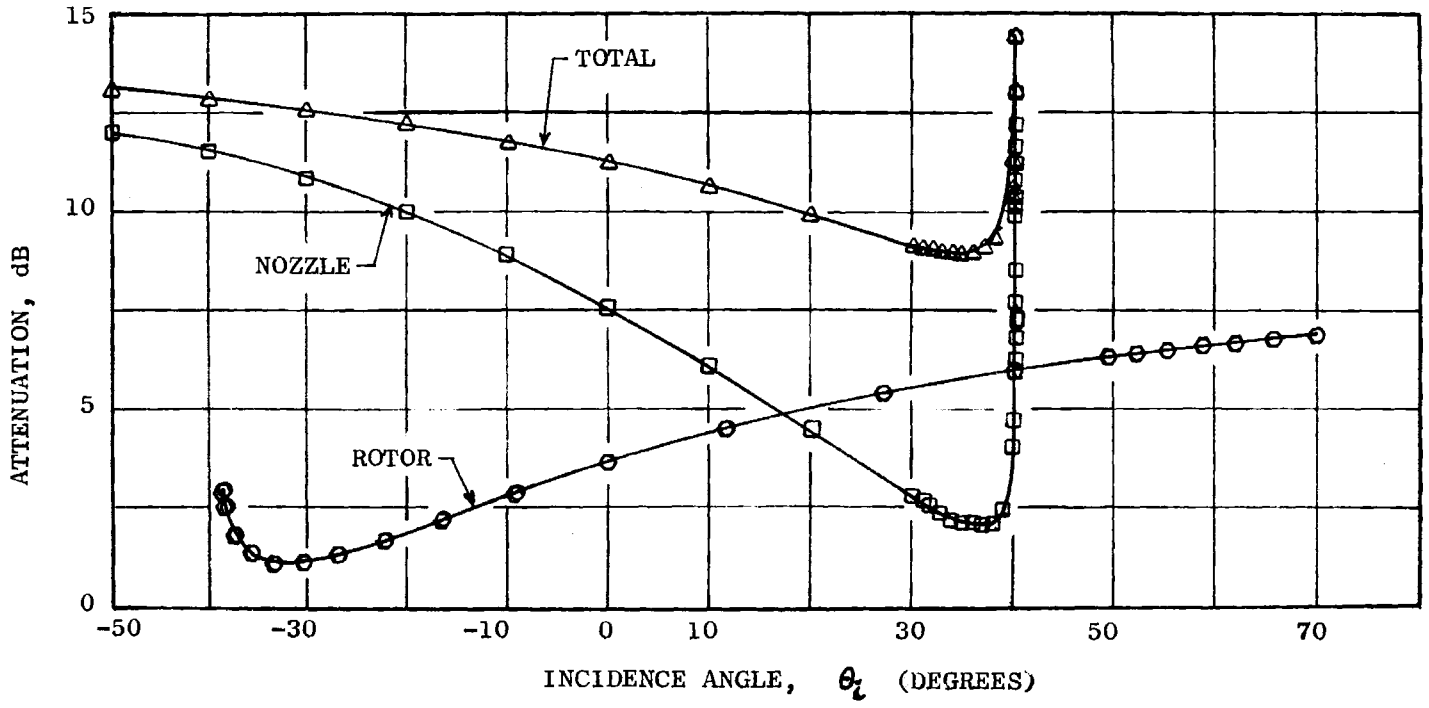

Figure 4-7. Stage 1 High Pressure Turbine, Low Frequency Attenuation.

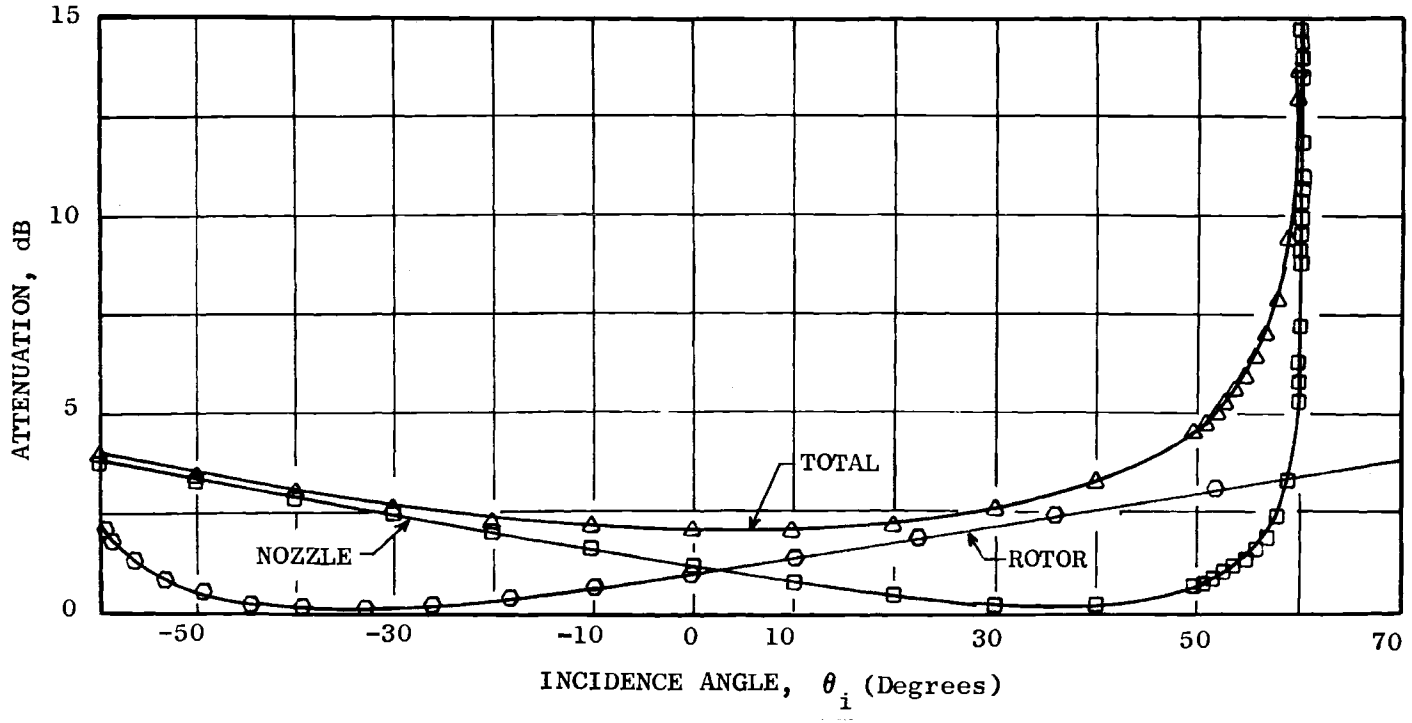

Figure 4-8. Stage 5 Low Pressure Turbine, Low Frequency Attenuation.

Table 4-1. Low Frequency Noise Attenuation for High Bypass Turbofan Engine Turbines.

Stage	Attenuation dB at zero degrees		
1	11.3		High
2	9.2		Pressure
			Turbine
1	5.2		
2	4.2		
3	4.0		Low
4	3.0		Pressure
5	2.0		Turbine
	38.9 dB	Total	

Table 4-2. Variation of Low Frequency Noise Attenuation with Speed.

% Fan RPM	Low Pressure Turbine Stage	Attenuation dB at zero degrees	
	1	5.0	
	2	3.8	
91	3	3.75	
	4	2.8	
	5	1.8	
		17.15	
	1	5.25	
	2	4.1	
88	3	3.8	
	4	2.8	
	5	1.9	
		17.85	
	1	5.0	
	2	3.8	
76	3	3.5	Approach
	4	3.5	Power
	5	1.5	
		17.3	
	1	4.9	
	2	3.6	
65	3	3.2	
	4	2.2	
	5	1.3	
		15.2	

SECTION 5.0

CONCLUSIONS

It is evident that more needs to be understood about the nature of the combustor noise source and the propagation path it follows through an engine before this prediction procedure can be refined further. Nevertheless, this prediction technique is quite good when the range of air flow rates (1 to 600 lb/sec) of the engine data which have been evaluated is considered. The important points in this report are tabulated here:

- The difference between component combustor levels and engine levels indicates attenuation along the propagation path through the engine.

- The overall power level prediction procedure using three lines for the engine classes is valid for the entire operating range. The data can be collapsed into a single line correlation by including a turbine work extraction term to account for the blade row attenuation.

- The spectral shapes of combustor and engine core noise vary somewhat but fall between the prediction spectrum and the spectral envelope.

- The frequency at which the spectrum peaks also varies, however, based on engine data the peak level occurs at 400 Hz $\pm$ a one-third octave band.

- The radiation directivity pattern was generally found to peak at 120° from the engine inlet.

REFERENCES

1. Motsinger, R.; "Prediction of Engine Combustor Noise and Correlation with T64 Engine Low Frequency Noise." General Electric Report, R72AEG313, October 1972.

2. Tedrick, R.N. and Kantarges, G.T.; "Small Turbine Engine Noise Reduction." Air Force Aero Propulsion Laboratory Report AF-APL-TR-73-79, Vol. IV, December 1973.

3. Bekofske, K.; "Attenuation of Acoustic Energy Across a Blade Row," General Electric Report 73CRD342, December 1973.

4. Emmerling, J.J.; "Experimental Clean Combustor Program Noise Measurement Addendum, Phase II Final Report," Contract Number NAS3-18551.

5. Gerend, R.P., Kumasaka, H.P., Roundhill, J.P. "Core Engine Noise" AIAA Paper No. 73-1027, October 1973.

APPENDIX A

THE ENGINE LOW FREQUENCY CORE NOISE PREDICTION

The procedure consists of first calculating the overall power level (OAPWL) from the prediction parameter. From that, the one-third octave band power levels are determined by imposing the prediction spectrum. These power levels, the arc radius, and the prediction directivity are finally used to calculate the one-third octave band sound pressure levels for any angle around the arc.

The overall power level correlation based on engine data was observed to form three separate but parallel prediction lines representing the three engine types: turbojet, turboshaft, and turbofan. The analysis for the attenuation of low frequency by turbine stages suggests that the work extraction by the turbines is a significant parameter[4] in this delineation of the engine types. The temperature drop across the turbines at design point was introduced into the correlation and a data collapse achieved as shown in Figure A-1. The prediction line is defined by:

$$\text{OAPWL} = 171 + 10 \log_{10} [\dot{W} (T_4-T_3)^2 (\rho_3/\rho_o)^2] - 10 \log (T_4-T_5)^4_{\text{Des.}} \qquad \text{(A-1)}$$

where $\dot{W}$ is the weight flow rate in lb/sec., T denotes the total temperature in degrees Rankine, and ρ the density; station 0 is ambient, 3 the combustor inlet, 4 the combustor exit, and 5 the low pressure turbine exit. The design point (T_4-T_5) must be used for any engine, regardless of the power setting.

Actually, the best mean square fit to the data of Figure A-1 is provided by a line with slope of 1.05 instead of the slope of 1.00 as used in equation (A-1). However, the difference between the two lines is very small, about 1 dB at either extreme, and the standard deviation is about 2.6 for both. Since either line is well within the scatter range of the other, the final choice was made on the basis of understanding the causation: the prediction parameter being a product of the heat release rate [$10 \log \dot{W}(T_4-T_3)$] and the thermo-acoustic efficiency [$10 \log (T_4-T_3)$].

The temperature drop term is related to the turbine pressure ratio which has previously been used in correlations by Gerend, et al.[5] and Grande[6]. The number of turbine stages cannot be recommended for use in a correlation as the analysis strongly indicates that this is not a linear dependency (see Table 4-1). The effects of the off-design performance on the turbine attenuation and nozzle termination are as yet largely unknown factors. Some investigation of these effects is being conducted under contracts NAS3-19435 and DOT-FA75WA-3688. Meanwhile, equation (A-1) is recommended for predicting the OAPWL.

The peak level of the prediction spectrum (Figure A-2) is given by:

$$\text{Peak PWL} = \text{OAPWL} - 6.8, \text{ dB} \qquad \text{(A-2)}$$

This sets the level of the peak frequency one-third octave band power spectrum. The peak frequency is nominally set at 400Hz, although it is realized that it may occur at a one-third octave band to either side, that is at 315 or 500 Hz.

The complete power level spectrum is defined by utilizing the narrow (T64) prediction spectrum of Figure A-2 with the peak PWL. However, if a degree of conservatism is desired, the broader spectrum envelope shown in Figure A-2 can be used insteady.

The sound pressure level at any point around the arc can be found from the power levels through:

$$\text{SPL} = \text{PWL} - 20 \text{ Log } R - 9.25 + \text{DI} - \text{AA} \qquad \text{(A-3)}$$

Where R is the arc radius in feet and DI is the directivity index from Figure A-3, and AA is the air attenuation.

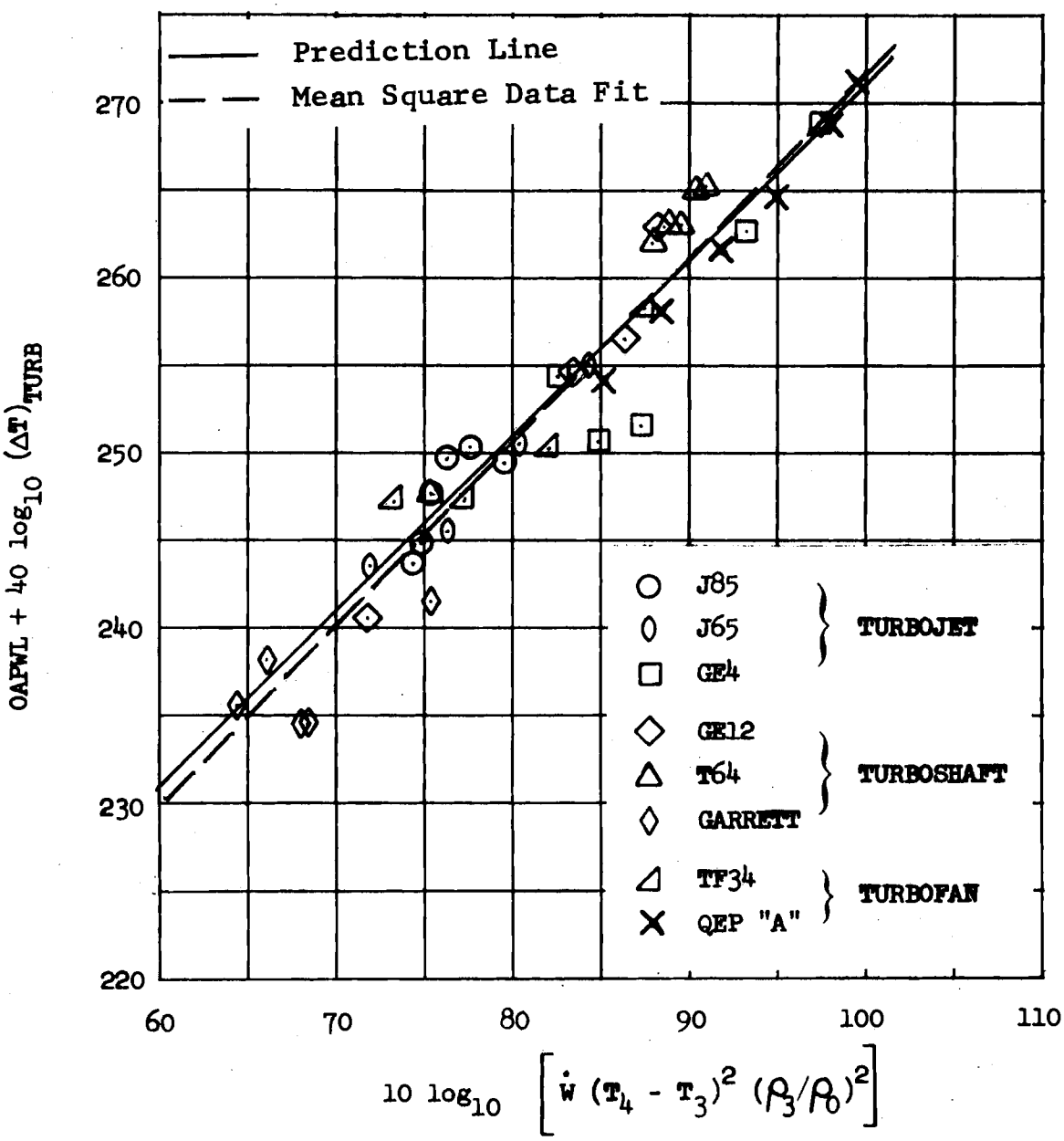

Figure A-1. Correlation for Core Noise Power Level.

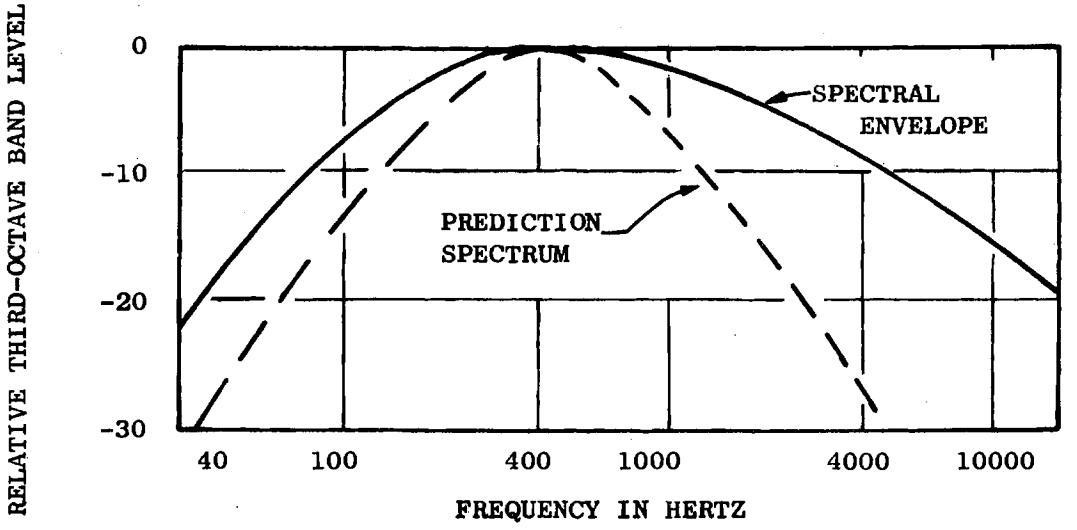

Figure A-2. Core Noise Prediction Spectra.

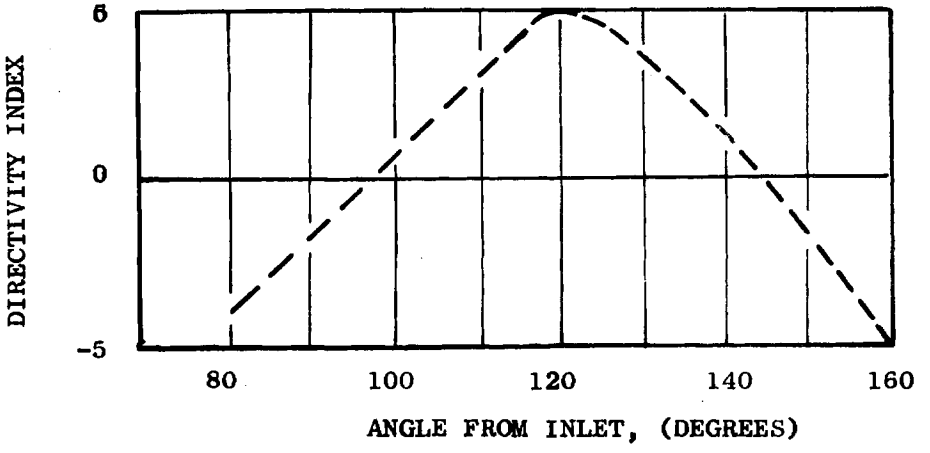

Figure A-3. Average Value of Directivity.

APPENDIX B

PROGRAM LISTING - PREDICTION OF BLADE ROW ATTENUATION

```
$LIST TADMA
12/11/73    11:37

00010 REAL K1, K2, KRA, KXØVKY, M1, M2, M1A, M2A, M1T, M2T
00020 REAL M3A, M4A, M3T, M4T
00030 DIMENSIØN QQ(100), ATTEN2(100), QQSAVE(100)
00040 PI=3.1415927 ;GRAV=32.17405 ;CØNV=778.26
00050 GAMMA=1.32 ;RGC=0.06854
00060 PRINT:"ABSØLUTE VELØCITIES ARE INPUT IN ØPTIØN 1"
00070 PRINT:"RELATIVE MACH NUMBERS ARE INPUT IN ØPTIØN 2"
00080 PRINT:"SELECT ØPTIØN 1 ØR 2  " ;READ: INPUT
00090 IF(INPUT .EQ. 2) GØ TØ 130
00100 PRINT:"ABSØLUTE VELØCITIES ARE IN FEET/SECØND" ;PRINT 1460
00110 PRINT:"ABSØLUTE FLØW ANGLES ARE IN DEGREES RELATIVE TØ FACE PLANE"
00120 PRINT:"  AND NEGATIVE IF FLØW DIRECTIØN ØPPØSITE WHEEL RØTATIØN"
00130 130 PRINT 1460 ;PRINT:"PRESSURES ARE IN PSIA"
00140 PRINT 1460 ;PRINT:"TEMPERATURES ARE IN DEGREES RANKINE"
00150 150 N=0 ;PRINT 1460
00160 DØ 170 I=1,100,1
00170 170 ATTEN2(I)=0.
00180 IF(INPUT .EQ. 2) GØ TØ 290
00190 PRINT:"INPUT DATA UPSTREAM ØF NØZZLE"
00200 PRINT:"AXIAL VELØCITY, ABSØLUTE FLØW ANGLE" ;READ: V1A,PSI1
00210 PRINT:"STATIC PRESSURE, TØTAL TEMPERATURE" ;READ: PS1,TZ1
00220 PRINT:"INPUT DATA BETWEEN NØZZLE AND BUCKET"
00230 PRINT:"AXIAL VELØCITY, ABSØLUTE FLØW ANGLE" ;READ: V2A,PSI2
00240 PRINT:"STATIC PRESSURE, TØTAL TEMPERATURE" ;READ: PS2,TZ2
00250 PRINT:"INPUT DATA DØWNSTREAM ØF BUCKET"
00260 PRINT:"AXIAL VELØCITY, ABSØLUTE FLØW ANGLE" ;READ: V3A, PSI3
00270 PRINT:"STATIC PRESSURE, TØTAL TEMPERATURE" ;READ:PS3, TZ3
00280 PRINT:"INPUT WHEEL SPEED(FPS)" ;READ: UW23 ;UW=0.
00290 290 IF(INPUT .EQ. 1) GØ TØ 420
00300 PRINT:"INPUT DATA UPSTREAM ØF NØZZLE"
00310 PRINT:"AXIAL AND TANGENTIAL RELATIVE MACH NUMBERS";READ:M1A,M1T
00320 PRINT:"STATIC TEMPERATURE AND PRESSURE" ;READ: TEMP1,PS1
00330 PRINT:"INPUT DATA DØWNSTREAM ØF NØZZLE"
00340 PRINT:"AXIAL AND TANGENTIAL RELATIVE MACH NUMBERS";READ:M2A,M2T
00350 PRINT:"STATIC TEMPERATURE AND PRESSURE" ;READ: TEMP2,PS2
00360 PRINT:"INPUT DATA UPSTREAM ØF BUCKET"
00370 PRINT:"AXIAL AND TANGENTIAL RELATIVE MACH NUMBERS";READ:M3A,M3T
00380 TEMP3=TEMP2 ;PS3=PS2
00390 PRINT:"INPUT DATA DØWNSTREAM ØF BUCKET"
00400 PRINT:"AXIAL AND TANGENTIAL RELATIVE MACH NUMBERS";READ:M4A,M4T
00410 PRINT:"STATIC TEMPERATURE AND PRESSURE" ;READ: TEMP4,PS4
00420 420 IF(INPUT .EQ. 2) GØ TØ 440
00430 PSI1=PI*PSI1/180. ;PSI2=PI*PSI2/180. ;PSI3=PI*PSI3/180.
00440 440 N=N+1 ;IF(INPUT .EQ. 2) GØ TØ 530
00450 V1T=V1A/TAN(PSI1) ;V2T=V2A/TAN(PSI2)
00460 V1=SQRT(V1A*V1A+V1T*V1T) ;V2=SQRT(V2A*V2A+V2T*V2T)
00470 W1A=V1A ;W2A=V2A ;W1T=V1T-UW ;W2T=V2T-UW
00480 W1=SQRT(W1A*W1A+W1T*W1T) ;W2=SQRT(W2A*W2A+W2T*W2T)
00490 AZ1=SQRT(GAMMA*GRAV*RGC*CØNV*TZ1)
00500 AZ2=SQRT(GAMMA*GRAV*RGC*CØNV*TZ2)
```

```
00510 TEMP1=TZ1*(1.-(GAMMA-1.)*(V1A*V1A+V1T*V1T)/(2.*AZ1*AZ1))
00520 TEMP2=TZ2*(1.-(GAMMA-1.)*(V2A*V2A+V2T*V2T)/(2.*AZ2*AZ2))
00530 530 A1=SQRT(GAMMA*GRAV*RGC*CØNV*TEMP1)
00540 A2=SQRT(GAMMA*GRAV*RGC*CØNV*TEMP2)
00550 ARA=A1/A2 ;KRA=1./ARA
00560 IF(INPUT .EQ. 2) GØ TØ 580
00570 M1A=W1A/A1 ;M2A=W2A/A2 ;M1T=W1T/A1 ;M2T=W2T/A2
00580 580 M1=SQRT(M1A*M1A+M1T*M1T) ;M2=SQRT(M2A*M2A+M2T*M2T)
00590 QTC1=ATAN2(SQRT(1.-M2A*M2A), -M2A)
00600 QTC2=ATAN2(-SQRT(1.-M2A*M2A), -M2A)
00610 GTC1=SIN(QTC1)/(KRA*(1.+M2A*CØS(QTC1)+M2T*SIN(QTC1)))
00620 GTC2=SIN(QTC2)/(KRA*(1.+M2A*CØS(QTC2)+M2T*SIN(QTC2)))
00630 GTC=GTC1 ;QTC=QTC1 ;M=0
00640 640 M=M+1 ;QQTC=180.*QTC/PI
00650 ATC=(1.-GTC*M1T)*(1.-GTC*M1T)-GTC*GTC
00660 BTC=-2.*GTC*M1A*(1.-GTC*M1T)
00670 CTC=-GTC*GTC*(1.-M1A*M1A)
00680 X=BTC*BTC-4.*ATC*CTC
00690 IF(X .LT. 0.) GØ TØ 820
00700 DDTC=(-BTC-SIGN(1.,BTC)*SQRT(BTC*BTC-4.*ATC*CTC))/2.
00710 QC=ATAN2(DDTC,ATC) ;QQC=180.*QC/PI ;PRINT 1460
00720 IF(N .EQ. 2) GØ TØ 740
00730 PRINT:"NØZZLE ATTENUATIØN" ;PRINT 1460 ;GØ TØ 750
00740 740 PRINT:"BUCKET AND STAGE ATTENUATIØN" ;PRINT 1460
00750 750 PRINT:"UPSTREAM CUT-ØFF ØCCURS AT INCIDENCE ANGLES ØF"
00760 CUTØFF=90.+180.*ARSIN(M1A)/PI ;PRINT 1430, CUTØFF
00770 CUTØFF=-CUTØFF ;PRINT 1430, CUTØFF ;PRINT 1460
00780 PRINT:"DØWNSTREAM CUT-ØFF ØCCURS AT A TRANSMISSIØN ANGLE ØF"
00790 PRINT 1430, QQTC ;PRINT 1460
00800 PRINT:"THE CØRRESPØNDING INCIDENCE ANGLE IS"
00810 PRINT 1430, QQC ;PRINT 1460
00820 820 IF(M .EQ. 2) GØ TØ 840
00830 GTC=GTC2 ; QTC=QTC2 ; GØ TØ 640
00840 840 IF(M1 .LT. 1. .AND. M2 .LT. 1.) GØ TØ 860
00850 PRINT:"SUPERSØNIC RELATIVE FLØW" ;GØ TØ 1400
00860 860 IF(N .EQ. 1) GØ TØ 890
00870 PRINT:"  THETA   THETA T    T      V      R
00880 &    ATTEN ATTEN2  THETA I" ;GØ TØ 900
00890 890 PRINT:" THETA I  THETA T    T      V      R    ATTEN"
00900 900 RHØRA=PS1*TEMP2/(PS2*TEMP1)
00910 ALPHA=ATAN2(M1T,M1A) ;BETA=ATAN2(M2T,M2A)
00920 GØ TØ (930, 1050), N
00930 930 QQ(1)=90.+180.*ARSIN(M1A)/PI ;QQMIN=-QQ(1) ;S=10.
00940 QQHØLD=10.*AINT((QQ(1)+10.)/10.)
00950 IF(QQC .LT. 0.) GØ TØ 980
00960 QQ(1)=-90.-180.*ARSIN(M1A)/PI ;QQMAX=-QQ(1) ;S=-10.
00970 QQHØLD=10.*AINT((QQ(1)-10.)/10.)
00980 980 DØ 1040 J=2,100,1
00990 QQ(J)=QQHØLD-S ;QQHØLD=QQ(J)
01000 IF(ABS(QQ(J)-QQC) .LT. ABS(1.1*S)) S=0.1*S
01010 IF(ABS(S) .LT. 0.0001) GØ TØ 1050
01020 IF(QQC .LT. 0.) GØ TØ 1040
01030 IF(QQ(J) .GT. QQMAX) GØ TØ 1050
01040 1040 IF(QQ(J) .LT. QQMIN) GØ TØ 1050
01050 1050 DØ 1330 K=1,100,1
01060 IF(N .EQ. 1) QQSAVE(K)=QQ(K)
01070 IF(QQ(K) .LT. QQC .AND. N .EQ. 2) GØ TØ 1330
```

```
01080 IF(K .EQ. (J+1)) GØ TØ 1340
01090 Q=PI*QQ(K)/180.
01100 IF(ABS(QQ(K)) .GT. 0.001) GØ TØ 1110 ;KXØVKY=100000. ;GØ TØ 1120
01110 1110 KXØVKY=((1.+M1A*CØS(Q)+M1T*SIN(Q))/(KRA*SIN(Q))-M2T)/M2A
01120 1120 QR=ATAN((1.-M1A*M1A)*SIN(Q)/((1.+M1A*M1A)*CØS(Q)+2.*M1A))
01130 G=KRA*SIN(Q)/(1.+M1A*CØS(Q)+M1T*SIN(Q))
01140 A=(1.-G*M2T)*(1.-G*M2T)-G*G ;B=-2.*G*M2A*(1.-G*M2T)
01150 C=-G*G*(1.-M2A*M2A) ;DD=(-B-SIGN(1.,B)*SQRT(B*B-4.*A*C))/2.
01160 QT=ATAN2(DD,A) ;QQT=180.*QT/PI
01170 T1=ARA*(M2A+CØS(QT)) ;V1=ARA ;R1=CØS(QR)-M1A ;C1=M1A+CØS(Q)
01180 T2=RHØRA*(1.+M2*CØS(BETA-QT)) ;V2=RHØRA*(M2A-KXØVKY*M2T)
01190 R2=M1*CØS(ALPHA+QR)-1. ;C2=1.+M1*CØS(ALPHA-Q)
01200 T3=SIN(QT-BETA) ;V3=-(SIN(BETA)+KXØVKY*CØS(BETA)) ;R3=0.;C3=0.
01210 D= T1*V2*R3+V1*R2*T3+R1*T2*V3-R1*V2*T3-T1*R2*V3-V1*T2*R3
01220 T=(C1*V2*R3+V1*R2*C3+R1*C2*V3-R1*V2*C3-C1*R2*V3-V1*C2*R3)/D
01230 V=(T1*C2*R3+C1*R2*T3+R1*T2*C3-R1*C2*T3-T1*R2*C3-C1*T2*R3)/D
01240 R=(T1*V2*C3+V1*C2*T3+C1*T2*V3-C1*V2*T3-T1*C2*V3-V1*T2*C3)/D
01250 V1A=M1A*A1 ;V1T=M1T*A1 ;V2A=M2A*A2 ;V2T=M2T*A2
01260 Z1=(A1+V1A*CØS(Q)+V1T*SIN(Q))*(A1*CØS(Q)+V1A)
01270 Z2=(A2+V2A*CØS(QT)+V2T*SIN(QT))*(A2*CØS(QT)+V2A)
01280 ATTEN=-4.342945*ALØG(T*T*RHØRA*ARA*ARA*ARA*ABS(Z2/Z1))
01290 ATTEN2(K)=ATTEN2(K)+ATTEN
01300 GØ TØ (1310,1320),N
01310 1310 PRINT 1450,QQ(K),QQT,T,V,R,ATTEN ;GØ TØ 1330
01320 1320 PRINT 1440, QQ(K),QQT,T,V,R,ATTEN,ATTEN2(K),QQSAVE(K)
01330 1330 QQ(K)=QQT
01340 1340 GØ TØ (1350, 1400),N
01350 1350 IF(INPUT .EQ. 2) GØ TØ 1380
01360 V1A=V2A ;V2A=V3A ;PSI1=PSI2 ;PSI2=PSI3
01370 PS1=PS2 ;PS2=PS3 ;TZ1=TZ2 ;TZ2=TZ3 ;UW=UW23 ;GØ TØ 440
01380 1380 M1A=M3A ;M2A=M4A ;M1T=M3T ;M2T=M4T
01390 TEMP1=TEMP3 ;TEMP2=TEMP4 ;PS1=PS3 ;PS2=PS4 ;GØ TØ 440
01400 1400 PRINT 1460
01410 PRINT: "MØRE INPUT? (YES=1, NØ=2)  " ;READ: MØRE
01420 GØ TØ (150, 1470), MØRE
01430 1430 FØRMAT(F10.3)
01440 1440 FØRMAT(2F9.3, 5F7.3, F9.3)
01450 1450 FØRMAT(2F9.3, 4F7.3)
01460 1460 FØRMAT(/)
01470 1470 END
```